Meccanica (2016) 51:2059–2098
DOI 10.1007/s11012-016-0361-y

3D exact and 2D generalized differential quadrature models for free vibration analysis of functionally graded plates and cylinders

S. Brischetto · F. Tornabene · N. Fantuzzi · E. Viola

Received: 21 July 2015 / Accepted: 4 January 2016 / Published online: 19 January 2016

Abstract The paper proposes a comparison between a three-dimensional (3D) exact solution and several two-dimensional (2D) numerical solutions. Numerical methods include classical 2D finite elements (FEs), and classical and refined 2D generalized differential quadrature (GDQ) solutions. The free vibration analysis of two different configurations of functionally graded material (FGM) plates and cylinders is proposed. The first configuration considers a one-layered FGM structure. The second one is a sandwich configuration with external classical skins and an internal FGM core. Low and high order frequencies are analyzed for thick and thin simply supported structures. Vibration modes are investigated to make a comparison between results obtained via the 2D numerical methods and those obtained by means of the 3D exact solution. The 3D exact solution is based on the differential equations of equilibrium written in general orthogonal curvilinear coordinates. This exact method is based on a layer-wise approach where the continuity of displacements and transverse shear/normal stresses is imposed at the interfaces between the layers of the structure. The 2D finite element results are obtained by means of a well-known commercial FE code. Classical and refined 2D GDQ models are based on a generalized unified approach which considers both equivalent single layer and layer-wise theories. The differences between 2D numerical solutions and 3D exact solutions depend on the considered mode, the order of frequency, the thickness ratio of the structure, the geometry, the embedded material and the lamination sequence.

Keywords Functionally graded materials · Plates · Cylinders · Finite element method · Exact three-dimensional solution · Two-dimensional solutions · Generalized differential quadrature method · Free vibrations · Vibration modes

S. Brischetto (✉)
Department of Mechanical and Aerospace Engineering, Politecnico di Torino, corso Duca degli Abruzzi, 24, 10129 Turin, Italy
e-mail: salvatore.brischetto@polito.it

F. Tornabene · N. Fantuzzi · E. Viola
DICAM Department, University of Bologna, Bologna, Italy

1 Introduction

In Functionally Graded Materials (FGMs) two or more constituent phases have a continuously variable composition through a particular direction [1, 2]. FGMs are a new generation of composite materials with a number of advantages such as a potential reduction of in-plane and transverse through-the-thickness stresses, an improved residual stress distribution, enhanced thermal properties, higher fracture toughness, and reduced stress intensity factors [3, 4]. In the design of sandwich structures, the use of FGM cores is a valid alternative to classical cores because they allow the continuity of in-plane stresses in

the thickness direction that sandwiches embedding conventional cores do not have [5, 6]. The severe temperature loads involved in many engineering applications, such as thermal barrier coatings, engine components or rocket nozzles, require high-temperature resistant materials and high structural performance. The use of FGM structures embedding ceramic and metallic phases that continuously vary through the thickness direction could be an optimal solution for these applications [7]. Further FGM applications were described in [8] where these materials were used to reproduce biological structures characterized by functional spatially distributed gradients in which each layer has one or more specific functions to perform. FGMs require an accurate evaluation of displacements, strains, stresses and vibrations. These variables are fundamental in the design of FGM structures. For these reasons, several refined 2D [11, 12] and 3D models have been developed for the analysis of plate and shell elements embedding functionally graded layers. A thorough introduction about some applications of FGM plates and shells in the literature can be found in the recent review papers [9, 10].

In the literature, three-dimensional solutions for FGM structures are given for specific geometries separately and not in a general framework for different geometries such as plates, cylindrical or spherical shells [13]. Dong [14] investigated three-dimensional free vibrations of functionally graded annular plates with different boundary conditions using the Chebyshev–Ritz method. Li et al. [15] analyzed free vibrations of functionally graded material sandwich rectangular plates using the Chebyshev–Ritz method too. A semi-analytical approach composed of differential quadrature method (DQM) and series solution was adopted in Malekzadeh [16] to solve the equations of motions for the free vibration analysis of thick FGM plates supported on two-parameter elastic foundation. Further three-dimensional models for free vibration analysis of FGM plates used a closed exact solution [17, 18]. Other three-dimensional exact models allow static analysis of FGM plates. Kashtalyan [19] and Xu and Zhou [20] showed the bending of one-layered functionally graded plates. Kashtalyan and Menshykova [21] investigated the bending of sandwich plates embedding FGM cores. Zhong and Shang [22] developed an exact three-dimensional analysis for a functionally gradient piezoelectric rectangular plate that was simply supported and grounded along its four edges. Further works analyze FGM shells. Alibeigloo et al. [23] investigated 3D free vibrations of a functionally graded cylindrical shell embedded in piezoelectric layers. An analytical method for simply supported boundary conditions and a semi-analytical method for non-simply supported conditions were used. Zahedinejad et al. [24] studied free vibration analysis of functionally graded (FG) curved thick panels under various boundary conditions using the three-dimensional elasticity theory and the differential quadrature method. The trigonometric functions were used to discretize the governing equations. Chen et al. [25] proposed free vibrations of simply supported, fluid-filled cylindrically orthotropic functionally graded shells with arbitrary thickness. A laminate approximate model was employed, it is suitable for an arbitrary variation of material constants along the radial direction. An exact elasticity solution was presented in [26] for the free and forced vibrations of functionally graded cylindrical shells. Three-dimensional linear elastodynamics equations were used and they were simplified to the case of generalized plane strain deformation in the axial direction. A meshless method based on the local Petrov-Galerkin approach was presented for three-dimensional (3-D) axisymmetric linear elastic solids with continuously varying material properties for the cases of 3D stress analysis of FGM bodies [27], 3D heat conduction analysis of FGM bodies [28], and 3D static and elastodynamic analysis of FGM bodies [29].

It has been demonstrated that an accurate and reliable numerical approach for solving partial differential systems of equations is the Generalized Differential Quadrature (GDQ) method, that belongs to the family of collocation methods and solves the mathematical problem on structured points located on the structure [30]. Interesting works about the two-dimensional GDQ solution for the analysis of FGM plates and shells can be found in [31–37]. Static analysis of FGM structures have been investigated in [31, 32]. The investigation of the free vibration of shells on Winkler-Pasternak foundation can be found in [33, 34]. Further general works about GDQ method and FGMs can be found in [35–37].

The present paper proposes a free vibration analysis of simply-supported one-layered and sandwich FGM plates and cylinders. Low and high frequencies and related modes are investigated. The importance of higher order frequency investigation has been extensively discussed in the reports by Leissa [38, 39], in the book by Werner [40] and in the work by Brischetto and Carrera [41].

The main aim of this work is the comparison between the results obtained by means of an exact three-dimensional (3D) solution, and those obtained by means of the classical two-dimensional (2D) finite element method (FEM) and by means of the classical and refined 2D generalized differential quadrature (GDQ) models. It is an extension of the previous authors' work about the analysis of multilayered composite and sandwich cylindrical and spherical shell panels [42]. The proposed exact 3D solution was developed by Brischetto in [13, 42–47], where the differential equations of equilibrium written in general orthogonal curvilinear coordinates were exactly solved by means of the exponential matrix method. The 2D FE results were obtained by means of the commercial finite element code Patran and Nastran [48]. The 2D modeling of FGM plates and shells has been proposed, by the authors, for different structural components. First order shear deformation theory (GDQ-RM) has been extended to plates, revolution shells and doubly-curved shells in [49–54]. A unified formulation for high order 2D models has been introduced for the free vibration problem of laminated FGM and laminated composite structures in [55, 56], respectively. As far as the static problem of FGM shells is concerned, preliminary results were published in [57, 58], where a stress recovery procedure has been implemented to calculate the stress and strain behaviors through the shell thickness. The same approach has been extended to high order 2D models in [59, 60] where sandwich composites have been accurately analyzed.

In the most general case of exact three-dimensional analyses, the number of frequencies for a free vibration problem is infinite: three displacement components (3 degrees of freedom DOF) in each point (points are ∞ in the 3 directions x, y, z) leads to $3 \times \infty^3$ vibration modes. Assumptions are made in the thickness direction z in the case of a 2D plate/shell model, the three displacements in each point are expressed in terms of a given number of degrees of freedom (NDOF) through the thickness direction z. NDOF varies from theory to theory. As a result, the number of vibration modes is $NDOF \times \infty^2$ in the case of exact 2D models. For exact 1D beam models, the number of vibration modes is $NDOF \times \infty^1$. In the case of 2D computational models, such as the Finite Element (FE) method or the generalized differential quadrature (GDQ) models, the number of modes is a finite number. This number coincides with the total number of employed degrees of freedom: $\sum_1^{Node} NDOF_i$, where $Node$ denotes the number of nodes used in the FE mathematical model or in the GDQ analysis, and $NDOF_i$ is the NDOF through the thickness direction z in the i-node. It is clear that some modes cannot be calculated by simplified models (such as computational two-dimensional models) [41]. In order to make a comparison between the 2D FE free vibration results, the 2D GDQ results and the 3D exact free vibration results, the investigation of the vibration modes is mandatory in order to understand which frequencies must be compared.

In the literature review proposed in this introduction, only a few works analyzed higher order frequencies for FGM structures. Moreover, papers that discuss the comparison between numerical 2D models and exact 3D models are even less frequent. The present work aims to fill this gap, it compares the free frequencies for FGM plates and cylinders obtained by means of the commercial FE code Nastran, the classical and refined 2D GDQ models, and the exact 3D solution. The proposed 3D exact solution gives results for plates, cylindrical and spherical shell panels, and cylindrical closed shells. However, the comparison with the commercial FE code and the GDQ models is proposed only for plates and cylinders for the sake of brevity. A future work will also consider the free frequency analysis of FGM cylindrical and spherical shells by means of 3D exact and 2D numerical models. The aim of the present paper is to understand how to compare these three different methods (exact 3D and numerical FE and GDQ solutions) and also to show the limitations of classical 2D theories.

2 Exact three-dimensional model

Three-dimensional linear elastic constitutive equations in orthogonal curvilinear coordinates (α, β, z) (see Fig. 1) are here given for a generic k isotropic layer. Coefficients C_{qr} depend on the thickness coordinate z in the case of functionally graded materials. The stress components ($\sigma_{\alpha\alpha}$, $\sigma_{\beta\beta}$, σ_{zz}, $\sigma_{\beta z}$, $\sigma_{\alpha z}$, $\sigma_{\alpha\beta}$) are linked with the strain components ($\epsilon_{\alpha\alpha}$, $\epsilon_{\beta\beta}$, ϵ_{zz}, $\gamma_{\beta z}$, $\gamma_{\alpha z}$, $\gamma_{\alpha\beta}$) for each k FGM layer as:

$$\sigma_{\alpha\alpha k} = C_{11k}(z)\epsilon_{\alpha\alpha k} + C_{12k}(z)\epsilon_{\beta\beta k} + C_{13k}(z)\epsilon_{zzk}, \quad (1)$$

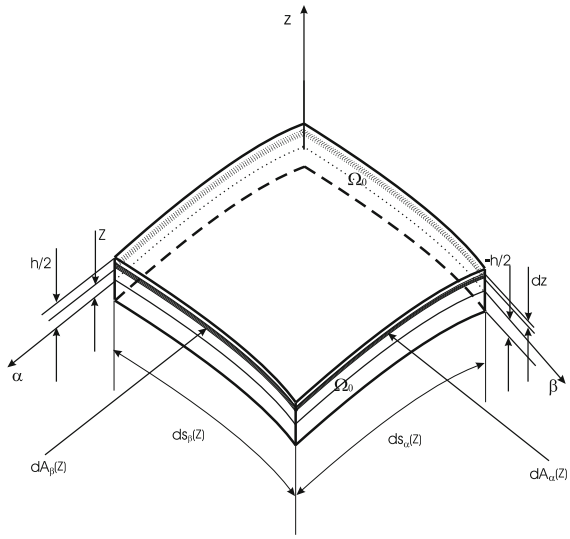

Fig. 1 Geometry, notation and reference system for shells

$$\sigma_{\beta\beta k} = C_{12k}(z)\epsilon_{\alpha\alpha k} + C_{22k}(z)\epsilon_{\beta\beta k} + C_{23k}(z)\epsilon_{zzk}, \quad (2)$$

$$\sigma_{zzk} = C_{13k}(z)\epsilon_{\alpha\alpha k} + C_{23k}(z)\epsilon_{\beta\beta k} + C_{33k}(z)\epsilon_{zzk}, \quad (3)$$

$$\sigma_{\beta zk} = C_{44k}(z)\gamma_{\beta zk}, \quad (4)$$

$$\sigma_{\alpha zk} = C_{55k}(z)\gamma_{\alpha zk}, \quad (5)$$

$$\sigma_{\alpha\beta k} = C_{66k}(z)\gamma_{\alpha\beta k}. \quad (6)$$

The strain-displacement relations of three-dimensional theory of elasticity in orthogonal curvilinear coordinates, as also shown in [38, 39, 61], are here written for the generic k layer of the multilayered FGM shell with constant radii of curvature (see Fig. 1):

$$\epsilon_{\alpha\alpha k} = \frac{1}{H_\alpha}\frac{\partial u_k}{\partial\alpha} + \frac{w_k}{H_\alpha R_\alpha}, \quad (7)$$

$$\epsilon_{\beta\beta k} = \frac{1}{H_\beta}\frac{\partial v_k}{\partial\beta} + \frac{w_k}{H_\beta R_\beta}, \quad (8)$$

$$\epsilon_{zzk} = \frac{\partial w_k}{\partial z}, \quad (9)$$

$$\gamma_{\beta zk} = \frac{1}{H_\beta}\frac{\partial w_k}{\partial\beta} + \frac{\partial v_k}{\partial z} - \frac{v_k}{H_\beta R_\beta}, \quad (10)$$

$$\gamma_{\alpha zk} = \frac{1}{H_\alpha}\frac{\partial w_k}{\partial\alpha} + \frac{\partial u_k}{\partial z} - \frac{u_k}{H_\alpha R_\alpha}, \quad (11)$$

$$\gamma_{\alpha\beta k} = \frac{1}{H_\alpha}\frac{\partial v_k}{\partial\alpha} + \frac{1}{H_\beta}\frac{\partial u_k}{\partial\beta}. \quad (12)$$

The parametric coefficients for shells with constant radii of curvature are:

$$H_\alpha = \left(1 + \frac{z}{R_\alpha}\right) = \left(1 + \frac{\tilde{z} - h/2}{R_\alpha}\right),$$
$$H_\beta = \left(1 + \frac{z}{R_\beta}\right) = \left(1 + \frac{\tilde{z} - h/2}{R_\beta}\right), \quad H_z = 1, \quad (13)$$

h is the total thickness of the structure. H_α and H_β depend on z or $\tilde{z}$ coordinate (see Fig. 2). $H_z = 1$ because z coordinate is always rectilinear. R_α and R_β are the principal radii of curvature along the coordinates α and β, respectively. Symbol ∂ indicates the partial derivatives. General geometrical relations for spherical shells in Eqs. (7)–(12) degenerate into geometrical relations for cylindrical shells when R_α or R_β is infinite (with H_α or H_β equals one). They degenerate into geometrical relations for plates when both R_α and R_β are infinite (with $H_\alpha = H_\beta = 1$) (further details can be found in [38, 39, 61]).

The three differential equations of equilibrium, written for the case of free vibration analysis of multilayered spherical shells with constant radii of curvature R_α and R_β, are here given (the most general form for variable radii of curvature can be found in [63, 64]):

$$H_\beta\frac{\partial\sigma_{\alpha\alpha k}}{\partial\alpha} + H_\alpha\frac{\partial\sigma_{\alpha\beta k}}{\partial\beta} + H_\alpha H_\beta\frac{\partial\sigma_{\alpha zk}}{\partial z} + \left(\frac{2H_\beta}{R_\alpha} + \frac{H_\alpha}{R_\beta}\right)\sigma_{\alpha zk} = \rho_k(z)H_\alpha H_\beta\ddot{u}_k, \quad (14)$$

$$H_\beta\frac{\partial\sigma_{\alpha\beta k}}{\partial\alpha} + H_\alpha\frac{\partial\sigma_{\beta\beta k}}{\partial\beta} + H_\alpha H_\beta\frac{\partial\sigma_{\beta zk}}{\partial z} + \left(\frac{2H_\alpha}{R_\beta} + \frac{H_\beta}{R_\alpha}\right)\sigma_{\beta zk} = \rho_k(z)H_\alpha H_\beta\ddot{v}_k, \quad (15)$$

$$H_\beta\frac{\partial\sigma_{\alpha zk}}{\partial\alpha} + H_\alpha\frac{\partial\sigma_{\beta zk}}{\partial\beta} + H_\alpha H_\beta\frac{\partial\sigma_{zzk}}{\partial z} - \frac{H_\beta}{R_\alpha}\sigma_{\alpha\alpha k} - \frac{H_\alpha}{R_\beta}\sigma_{\beta\beta k} + \left(\frac{H_\beta}{R_\alpha} + \frac{H_\alpha}{R_\beta}\right)\sigma_{zzk} = \rho_k(z)H_\alpha H_\beta\ddot{w}_k, \quad (16)$$

where $\rho_k(z)$ is the mass density that varies through the thickness of a functionally graded layer.

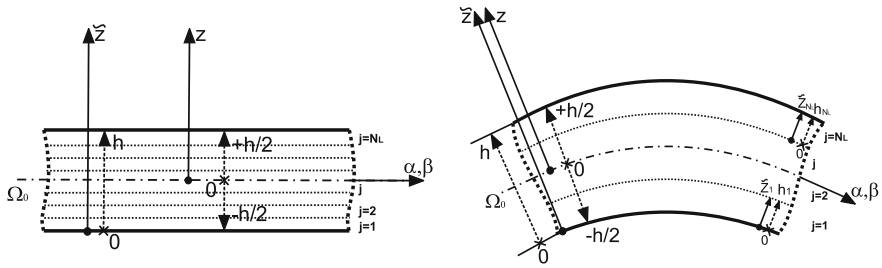

Fig. 2 Thickness coordinates and reference systems for plates and shells

$(\sigma_{\alpha\alpha k}, \sigma_{\beta\beta k}, \sigma_{zzk}, \sigma_{\beta zk}, \sigma_{\alpha zk}, \sigma_{\alpha\beta k})$ are the six stress components. $\ddot{u}_k$, $\ddot{v}_k$ and $\ddot{w}_k$ indicate the second temporal derivative of the three displacement components u_k, v_k and w_k, respectively. Each quantity depends on the k layer. R_α and R_β are referred to the mid-surface Ω_0 of the whole multilayered shell. H_α and H_β continuously vary through the thickness of the multilayered shell and they depend on the z thickness coordinate.

These equilibrium equations are valid for spherical shell panels and they degenerate in equilibrium equations for cylindrical open and closed shell panels when R_α or R_β is infinite (H_α or H_β equals 1), and in equilibrium equations for plates when R_α and R_β are infinite ($H_\alpha = H_\beta = 1$). Therefore, Eqs. (14)–(16) are valid for all the geometries indicated in Fig. 3.

The closed form of Eqs. (14)–(16) is obtained for simply supported shells and plates indicated in Fig. 3. The three displacement components have the following harmonic form:

$$u_j(\alpha,\beta,z) = U_j(z)e^{i\omega t}cos(\bar{\alpha}\alpha)sin(\bar{\beta}\beta), \tag{17}$$

$$v_j(\alpha,\beta,z) = V_j(z)e^{i\omega t}sin(\bar{\alpha}\alpha)cos(\bar{\beta}\beta), \tag{18}$$

$$w_j(\alpha,\beta,z) = W_j(z)e^{i\omega t}sin(\bar{\alpha}\alpha)sin(\bar{\beta}\beta), \tag{19}$$

where $U_j(z)$, $V_j(z)$ and $W_j(z)$ are the displacement amplitudes in α, β and z directions, respectively. i is the coefficient of the imaginary unit. $\omega = 2\pi f$ is the circular frequency where f is the frequency value, t is the time. In coefficients $\bar{\alpha} = \frac{m\pi}{a}$ and $\bar{\beta} = \frac{n\pi}{b}$, m and n are the half-wave numbers and a and b are the shell dimensions in α and β directions, respectively (calculated in the mid-surface Ω_0).

Equations (1)–(12) and (17)–(19) are introduced in Eqs. (14)–(16) in order to obtain the following system of equations for each j mathematical layer:

$$\begin{aligned}
&\left(-\frac{C_{55j}H_\beta}{H_\alpha R_\alpha^2} - \frac{C_{55j}}{R_\alpha R_\beta} - \bar{\alpha}^2\frac{C_{11j}H_\beta}{H_\alpha} \right.\\
&\left. -\bar{\beta}^2\frac{C_{66j}H_\alpha}{H_\beta} + \rho_j H_\alpha H_\beta \omega^2\right)U_j\\
&+\left(-\bar{\alpha}\bar{\beta}C_{12j} - \bar{\alpha}\bar{\beta}C_{66j}\right)V_j\\
&+\left(\bar{\alpha}\frac{C_{11j}H_\beta}{H_\alpha R_\alpha} + \bar{\alpha}\frac{C_{12j}}{R_\beta} + \bar{\alpha}\frac{C_{55j}H_\beta}{H_\alpha R_\alpha} + \bar{\alpha}\frac{C_{55j}}{R_\beta}\right)W_j\\
&+\left(\frac{C_{55j}H_\beta}{R_\alpha} + \frac{C_{55j}H_\alpha}{R_\beta}\right)U_{j,z}\\
&+\left(\bar{\alpha}C_{13j}H_\beta + \bar{\alpha}C_{55j}H_\beta\right)W_{j,z} + \left(C_{55j}H_\alpha H_\beta\right)U_{j,zz} = 0,
\end{aligned} \tag{20}$$

$$\begin{aligned}
&\left(-\bar{\alpha}\bar{\beta}C_{66j} - \bar{\alpha}\bar{\beta}C_{12j}\right)U_j\\
&+\left(-\frac{C_{44j}H_\alpha}{H_\beta R_\beta^2} - \frac{C_{44j}}{R_\alpha R_\beta} - \bar{\alpha}^2\frac{C_{66j}H_\beta}{H_\alpha} - \bar{\beta}^2\frac{C_{22j}H_\alpha}{H_\beta}\right.\\
&\left. +\rho_j H_\alpha H_\beta \omega^2\right)V_j + \left(\bar{\beta}\frac{C_{44j}H_\alpha}{H_\beta R_\beta} + \bar{\beta}\frac{C_{44j}}{R_\alpha} + \bar{\beta}\frac{C_{22j}H_\alpha}{H_\beta R_\beta}\right.\\
&\left. +\bar{\beta}\frac{C_{12j}}{R_\alpha}\right)W_j \quad + \left(\frac{C_{44j}H_\alpha}{R_\beta} + \frac{C_{44j}H_\beta}{R_\alpha}\right)V_{j,z}\\
&+\left(\bar{\beta}C_{44j}H_\alpha + \bar{\beta}C_{23j}H_\alpha\right)W_{j,z} + \left(C_{44j}H_\alpha H_\beta\right)V_{j,zz} = 0,
\end{aligned} \tag{21}$$

$$\begin{aligned}
&\left(\bar{\alpha}\frac{C_{55j}H_\beta}{H_\alpha R_\alpha} - \bar{\alpha}\frac{C_{13j}}{R_\beta} + \bar{\alpha}\frac{C_{11j}H_\beta}{H_\alpha R_\alpha} + \bar{\alpha}\frac{C_{12j}}{R_\beta}\right)U_j\\
&+\left(\bar{\beta}\frac{C_{44j}H_\alpha}{H_\beta R_\beta} - \bar{\beta}\frac{C_{23j}}{R_\alpha} + \bar{\beta}\frac{C_{22j}H_\alpha}{H_\beta R_\beta} + \bar{\beta}\frac{C_{12j}}{R_\alpha}\right)V_j\\
&+\left(\frac{C_{13j}}{R_\alpha R_\beta} + \frac{C_{23j}}{R_\alpha R_\beta} - \frac{C_{11j}H_\beta}{H_\alpha R_\alpha^2} - \frac{2C_{12j}}{R_\alpha R_\beta} - \frac{C_{22j}H_\alpha}{H_\beta R_\beta^2}\right.\\
&\left. -\bar{\alpha}^2\frac{C_{55j}H_\beta}{H_\alpha} - \bar{\beta}^2\frac{C_{44j}H_\alpha}{H_\beta} + \rho_j H_\alpha H_\beta \omega^2\right)W_j\\
&+\left(-\bar{\alpha}C_{55j}H_\beta - \bar{\alpha}C_{13j}H_\beta\right)U_{j,z}\\
&+\left(-\bar{\beta}C_{44j}H_\alpha - \bar{\beta}C_{23j}H_\alpha\right)V_{j,z}\\
&+\left(\frac{C_{33j}H_\beta}{R_\alpha} + \frac{C_{33j}H_\alpha}{R_\beta}\right)W_{j,z} + \left(C_{33j}H_\alpha H_\beta\right)W_{j,zz} = 0.
\end{aligned} \tag{22}$$

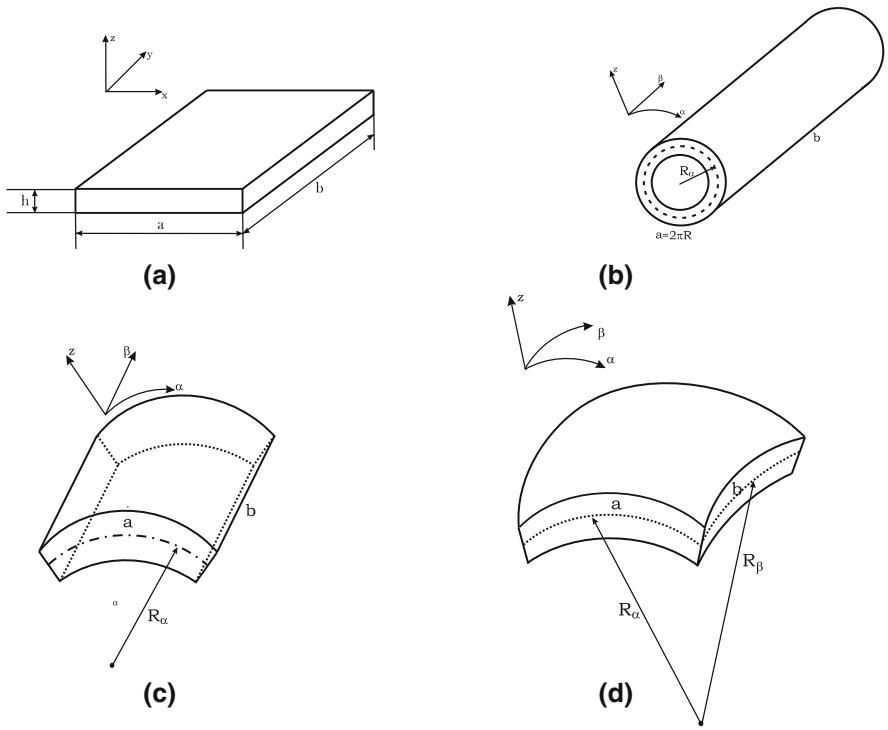

Fig. 3 Geometries for assessments and benchmarks

Elastic coefficients C_{qr} depend on the thickness coordinate z when the k layer is a functionally graded material layer. Parametric coefficients H_α and H_β depend on the thickness coordinate z in the case of shell geometry and they are equal 1 in case of plates. Therefore, Eqs. (20)–(22) do not have constant coefficients because of FGM layers and/or shell geometry. In order to obtain Eqs. (20)–(22) with constant coefficients, each k layer is divided in l mathematical layers where the coefficients C_{qr} can be assumed as constant and parametric coefficients H_α and H_β can be easily calculated in the middle of each mathematical layer. Equation (20)–(22) were rewritten by using $j = k \times l$ mathematical layers that allow constant coefficients to be considered (see [13] for further details).

Elastic coefficients and mass density can be assumed as constant in each j mathematical layer even if a functionally graded material is considered. Parametric coefficients H_α and H_β are also constant because the thickness coordinate z is known at the middle of each j layer. The system of Eqs. (20)–(22) is written in the following compact form using the nomenclature A_{sj} (with s from 1 to 19 and j from 1 to the N_L mathematical layer) for terms included in parentheses:

$$A_{1j}U_j + A_{2j}V_j + A_{3j}W_j + A_{4j}U_{j,z} + A_{5j}W_{j,z} + A_{6j}U_{j,zz} = 0, \tag{23}$$

$$A_{7j}U_j + A_{8j}V_j + A_{9j}W_j + A_{10j}V_{j,z} + A_{11j}W_{j,z} + A_{12j}V_{j,zz} = 0, \tag{24}$$

$$A_{13j}U_j + A_{14j}V_j + A_{15j}W_j + A_{16j}U_{j,z} + A_{17j}V_{j,z} + A_{18j}W_{j,z} + A_{19j}W_{j,zz} = 0. \tag{25}$$

Equations (23)–(25) are a system of three second order differential equations. They are written for spherical shell panels with constant radii of curvature but they automatically degenerate into equations for cylindrical shells and plates (see Fig. 3).

The system of second order differential equations can be reduced to a system of first order differential equations using the method described in [65, 66]. A compact form of the system of first order differential equations can be:

$$\boldsymbol{D}_j \frac{\partial \boldsymbol{U}_j}{\partial \tilde{z}} = \boldsymbol{A}_j \boldsymbol{U}_j, \tag{26}$$

where $\frac{\partial \boldsymbol{U}_j}{\partial \tilde{z}} = \boldsymbol{U}_j'$ and $\boldsymbol{U}_j = [U_j \; V_j \; W_j \; U_j' \; V_j' \; W_j']$. Equation (26) can be written as:

$$\boldsymbol{D}_j \boldsymbol{U}'_j = \boldsymbol{A}_j \boldsymbol{U}_j, \tag{27}$$

$$\boldsymbol{U}'_j = \boldsymbol{D}_j^{-1} \boldsymbol{A}_j \ \boldsymbol{U}_j, \tag{28}$$

$$\boldsymbol{U}'_j = \boldsymbol{A}_j^* \ \boldsymbol{U}_j, \tag{29}$$

with $\boldsymbol{A}_j^* = \boldsymbol{D}_j^{-1} \boldsymbol{A}_j$.

In the case of plate geometry, coefficients A_{3j}, A_{4j}, A_{9j}, A_{10j}, A_{13j}, A_{14j} and A_{18j} are zero because the radii of curvature R_α and R_β are infinite. The solution of Eq. (29) can be written as (see [66, 67]):

$$\boldsymbol{U}_j(\tilde{z}_j) = exp(\boldsymbol{A}_j^* \tilde{z}_j) \boldsymbol{U}_j(0) \quad \text{with} \quad \tilde{z}_j \in [0, h_j], \tag{30}$$

where $\tilde{z}_j$ is the thickness coordinate of each j layer from 0 at the bottom to h_j at the top (see Fig. 2). The exponential matrix is calculated with $\tilde{z}_j = h_j$ for each j layer as:

$$\boldsymbol{A}_j^{**} = exp(\boldsymbol{A}_j^* h_j) = \boldsymbol{I} + \boldsymbol{A}_j^* \, h_j + \frac{\boldsymbol{A}_j^{*2}}{2!} h_j^2 + \frac{\boldsymbol{A}_j^{*3}}{3!} h_j^3 + \cdots + \frac{\boldsymbol{A}_j^{*N}}{N!} h_j^N, \tag{31}$$

where $\boldsymbol{I}$ is the 6×6 identity matrix. This expansion has a fast convergence as indicated in [68] and it is not time consuming from the computational point of view. This method has already successfully applied by Messina [69] for the case of plates in rectlinear orthogonal coordinates (x, y, z) and by Soldatos and Ye [70] for the case of closed cylinders in cylindrical coordinates (ρ,θ).

Considering $j = N_L$ layers, $N_L - 1$ transfer matrices $\boldsymbol{T}_{j-1,j}$ must be calculated using for each interface the following conditions for interlaminar continuity of displacements and transverse shear/normal stresses:

$$u_j^b = u_{j-1}^t, \ \ v_j^b = v_{j-1}^t, \ \ w_j^b = w_{j-1}^t, \tag{32}$$

$$\sigma_{zzj}^b = \sigma_{zzj-1}^t, \ \ \sigma_{\alpha zj}^b = \sigma_{\alpha zj-1}^t, \ \ \sigma_{\beta zj}^b = \sigma_{\beta zj-1}^t, \tag{33}$$

that means each displacement and transverse stress component at the top (t) of the $j-1$ layer is equal to displacements and transverse stress components at the bottom (b) of the j layer.

The structures are simply supported and free stresses at the top and at the bottom of the whole multilayered shell, this feature means:

$$\sigma_{zz} = \sigma_{\alpha z} = \sigma_{\beta z} = 0 \quad \text{for} \quad z = -h/2, +h/2 \quad \text{or} \quad \tilde{z} = 0, h, \tag{34}$$

$$w = v = 0, \ \sigma_{\alpha\alpha} = 0 \quad \text{for} \quad \alpha = 0, a, \tag{35}$$

$$w = u = 0, \ \sigma_{\beta\beta} = 0 \quad \text{for} \quad \beta = 0, b. \tag{36}$$

Boundary conditions given by Eqs. (35) and (36) are identically satisfied by the displacement field in Eqs. (17)–(19). These boundary conditions do not take part to the determination of the maximal displacement amplitudes addressed in the remaining of the section.

All these conditions give the following final system:

$$\boldsymbol{E} \, \boldsymbol{U}_1(0) \ = \ \boldsymbol{0}, \tag{37}$$

where matrix $\boldsymbol{E}$ has always (6×6) dimension, independently from the number of layers N_L, even if the method uses a layer-wise approach. $\boldsymbol{U}_1(0)$ means $\boldsymbol{U}$ calculated at the bottom of the whole multilayered shell, first layer 1 with $\tilde{z}_1 = 0$. Further details about this procedure, and all the step missed in this paper can be found in [13, 42, 43] where the extensions of this 3D exact method have been made for the first time.

The free vibration analysis means to find the non-trivial solution of $\boldsymbol{U}_1(0)$ in Eq. (37) imposing the determinant of matrix $\boldsymbol{E}$ equals zero:

$$det[\boldsymbol{E}] = 0, \tag{38}$$

Equation (38) means to find the roots of an higher order polynomial in $\lambda = \omega^2$. For each pair of half-wave numbers (m, n) a certain number of circular frequencies (from I to ∞) are obtained. This number depends on the order N chosen for each exponential matrix $\boldsymbol{A}_j^{**}$ and the number N_L of mathematical layers.

A certain number of circular frequencies ω_s are found when half-wave numbers m and n are imposed in the structures. For each frequency ω_s, it is possible to find the vibration mode through the thickness in terms of the three displacement components. If the frequency ω_s is substituted in the (6×6) matrix $\boldsymbol{E}$, this last matrix has six eigenvalues. We are interested to the null space of matrix $\boldsymbol{E}$ that means to find the (6×1) eigenvector related to the minimum of the six eigenvalues proposed. This null space is the vector $\boldsymbol{U}$ calculated at the bottom of the whole structure for the chosen frequency ω_s:

$$\boldsymbol{U}_{1\omega_s}(0) = [U_1(0) \ \ V_1(0) \ \ W_1(0) \ \ U_1'(0) \ \ V_1'(0) \ \ W_1'(0)]_{\omega_s}^T, \tag{39}$$

T means the transpose of the vector and the subscript ω_s means that the null space is calculated for the circular frequency ω_s.

It is possible to find $\boldsymbol{U}_{j\omega_s}(\tilde{z}_j)$ (with the three displacement components $U_{j\omega_s}(\tilde{z}_j)$, $V_{j\omega_s}(\tilde{z}_j)$ and $W_{j\omega_s}(\tilde{z}_j)$ through the thickness) for each j layer of the multilayered structure using Eqs. (32)–(33) with the index j from 1 to N_L. The thickness coordinate $\tilde{z}$ can assume all the values from the bottom to the top of the structure.

2.1 Validation of the 3D exact model

Before the comparison study between the 3D exact solution and the several 2D numerical methods, the proposed 3D exact model has been validated by means of two comparisons with other 3D results already given in the literature. Further comparisons which validate the present 3D exact model can be found in [13, 42, 43].

The first assessment considers a simply supported square sandwich plate as proposed in Li et al. [15] (see geometry in Fig. 3a). The sandwich plate has two external skins with thickness $h_1 = h_3 = 0.1h$ and an internal core with thickness $h_2 = 0.8h$. The bottom skin is ceramic and the top skin is metallic. The core is made of a functionally graded material. Details about this configuration can be found in Fig. 4 and work [15]. The metallic (m) material has Young modulus $E_m =$ 70 GPa, mass density $\rho_m = 2707$ kg/m^3 and Poisson ratio $\nu_m = 0.3$. The ceramic (c) material has Young modulus $E_c = 380$ GPa, mass density $\rho_c = 3800$ kg/m^3 and Poisson ratio $\nu_c = 0.3$. The functionally graded core has constant Poisson ratio $\nu = 0.3$. Young modulus and mass density continuously vary through the thickness direction z as:

$$\begin{aligned} E(z) &= E_m + (E_c - E_m)V_c, \\ \rho(z) &= \rho_m + (\rho_c - \rho_m)V_c, \end{aligned} \tag{40}$$

where V_c is the volume fraction of the ceramic phase that continuously varies through the thickness as:

$$V_c = 1 - V_m = 1 - (0.5 + z/h_2)^p, \tag{41}$$

V_m is the volume fraction of metallic phase, z varies from $-h_2/2$ to $h_2/2$. Exponent p can assume values equal or greater than zero. Li et al. [15] propose a three-dimensional solution by means of the Ritz approach, and give the fundamental frequency for half-wave numbers $m = n = 1$ and for several thickness ratios a/h and exponents p. The circular frequencies are given in non-dimensional form $\bar{\omega} = \omega \frac{a^2}{h}\sqrt{\frac{\rho_0}{E_0}}$ with $E_0 = 1$ GPa and $\rho_0 = 1$ kg/m^3. Table 1 shows the comparison between the model proposed in Li et al. [15] and the present three-dimensional exact solution. The two methods are in accordance for each thickness ratio a/h and exponent p for the FGM law.

The second assessment considers a simply supported cylindrical shell panel as proposed in Zahedinejad et al. [24] (see geometry in Fig. 3c). The shell has the two dimensions a and b that are coincident ($a = b$), the thickness ratio investigated is a/h equals 5. Two different radii of curvature R_α are considered, that means a/R_α equals 0.5 or 1. The radius of curvature R_β is infinite. The shell is one-layered and it is made of a functionally graded material as shown in Fig. 4. In this case the structure is fully metallic at the bottom and fully ceramic at the top. This feature means that Eq. (40) is still valid, but the volume fraction of ceramic phase V_c is considered in the following form:

$$V_c = (0.5 + z/h)^p. \tag{42}$$

The metallic phase and the ceramic phase have the properties already seen for the first assessment [15]. The only difference is for ρ_m, which is equal to 2702 kg/m^3 (the first assessment considers $\rho_m = 2707$ kg/m^3). These material data can be found in Zahedinejad et al. [24], who propose a three-dimensional

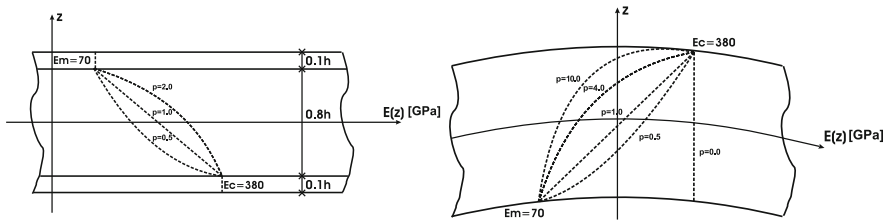

Fig. 4 Functionally graded material law through the thickness direction of the sandwich plate for assessment 1 (on the *left*) and the one-layered cylindrical shell panel for assessment 2 (on the *right*)

Table 1 First assessment for the 3D exact solution: sandwich plate with FGM core. Fundamental circular frequency $\bar{\omega}$ for half-wave numbers $m = n = 1$ and different thickness ratios a/h and exponents p for the material law

p	0.5	1.0	2.0	5.0	10
$a/h = 100$					
3D [15]	1.33931	1.38669	1.44491	1.53143	1.59105
Present 3D	1.33928	1.38671	1.44494	1.53148	1.59113
$a/h = 10$					
3D [15]	1.29751	1.34847	1.40828	1.49309	1.54980
Present 3D	1.29748	1.34848	1.40829	1.49311	1.54984
$a/h = 5$					
3D [15]	1.19580	1.25338	1.31569	1.39567	1.44540
Present 3D	1.19575	1.25337	1.31566	1.39564	1.44537

Table 2 Second assessment for the 3D exact solution: one-layered FGM cylindrical shell panel with thickness ratio $a/h = 5$. Fundamental circular frequency $\bar{\omega}$ for half-wave numbers $m = n = 1$ and different radii of curvature R_α and exponents p for the material law

p	0.0	0.5	1.0	4.0	10
$a/R_\alpha = 0.5$					
3D [24]	0.2113	0.1814	0.1639	0.1367	0.1271
Present 3D	0.2129	0.1817	0.1638	0.1374	0.1296
$a/R_\alpha = 1.0$					
3D [24]	0.2164	0.1852	0.1676	0.1394	0.1286
Present 3D	0.2155	0.1848	0.1671	0.1392	0.1300

differential quadrature method for the free vibration analysis of the cylindrical panel for imposed half-wave numbers $m = n = 1$ and for several exponent values p. The results are given as non-dimensional circular frequencies $\bar{\omega} = \omega h\sqrt{\frac{\rho_c}{E_c}}$. Table 2 shows that the present three-dimensional exact model gives results similar to those obtained with the method proposed by Zahedinejad et al. [24]. The minor differences are due to the fact that the present 3D model is given in exact form while the 3D model in Zahedinejad et al. [24] is proposed by means of a numerical method such as the differential quadrature method.

In the two proposed assessments, the present 3D solution uses $N_L = 100$ mathematical layers. The exponential matrix in Eq. (31) is approximated with order $N = 3$. The convergence of the approximation is very fast, a small N value is used because of the large number of layers N_L employed to correctly include the curvature effect and the gradation law of the material. The computational cost is low because the E matrix in Eq. (37) has always 6×6 dimension even if a layer wise approach is employed and $N_L = 100$ mathematical layers are used. The same values of N and N_L are also employed for benchmarks proposed in Sect. 5 where the present 3D solution is compared with several 2D numerical models.

After these two preliminary assessments, the present three-dimensional exact solution can be considered as validated for the free vibration analysis of one-layered and multilayered FGM plates and shells. The benchmarks in Sect. 5 will propose comparisons with 2D numerical models for plate and closed cylinder geometries. This choice is made for the sake of brevity. A future work will also consider FGM cylindrical and spherical shell panels.

3 2D finite element models

The 2D finite element results proposed in this paper have been obtained by means of the FE commercial code known as MSC Nastran & Patran [48]. Only simple geometries are analyzed in this paper (plates and cylinders). For these structures a maximum number of 5000 elements is sufficient for a correct convergence in the case of free vibration analysis (as it will be demonstrated in the section about the validation of the FE model). The 2D element employed in the free vibration analysis is the SHELL QUAD4 element of Nastran, it has four nodes for each element that are collocated in the four corners. The kinematic model used by Nastran in its 2D FEs is based on the Reissner–Mindlin hypotheses (equivalent single layer approach and

constant transverse displacement in the z direction). Nastran does not have any specified tool for the analysis of FGM structures, for this reason the FGM layer has been divided in a number N_L of j mathematical layers where the Young modulus and the mass density can be considered as constant and equal to the mean value of the jth layer. Figure 5 shows two examples for the approximation of the FGM properties (e.g., the Young modulus) through the thickness z. After a convergence study, 100 mathematical layers have been considered sufficient to correctly approximate all the FGM properties. Nastran has always been tested considering the FGM structures as multilayered structures with 100 mathematical layers with constant properties.

3.1 Validation of the finite element models

The FE model will be validated only for plates and cylinders because in Sect. 5 comparisons will be made only for these two geometries. This choice is due to the fact that we want to compare several laminations, materials and modes without lose in clarity and conciseness. The investigation for cylindrical and spherical panels could be the topic of a future work.

The FE code will be validated using the benchmarks which will be used in Sect. 5 where 2D numerical and 3D exact models will be compared. The description of these two main benchmarks follows.

The first geometry considered in this investigation is a simply supported square plate with dimensions

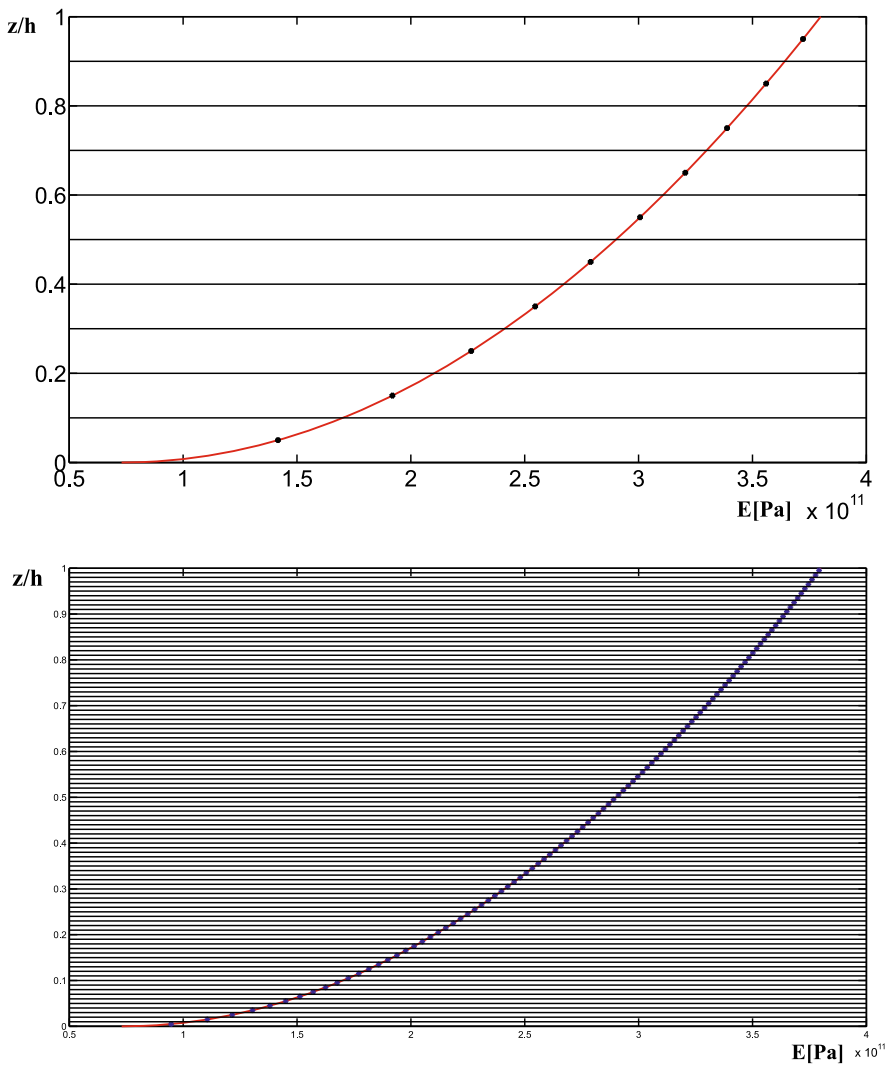

Fig. 5 Approximation of the FGM law with $p = 0.5$ through the thickness z by means of 10 mathematical layers (at the *top*) and 100 mathematical layers (at the *bottom*)

$a = b = 1$ m. Thickness values are $h = 0.1, 0.05, 0.01$ and 0.001 m that mean thickness ratios a/h = 10, 20, 100 and 1000, respectively (see Fig. 3a). The second geometry is a simply supported cylinder with radii of curvature $R_\alpha = 10$ m and $R_\beta = \infty$. The dimensions are $a = 2\pi R_\alpha$ and $b = 20$ m. The thickness values are $h = 0.01$, 0.1, 1 and 2 m that mean thickness ratios $R_\alpha/h = 1000$, 100, 10 and 5, respectively (see Fig. 3b). Both geometries will be considered as isotropic one-layered FGM ($h_1 = h$) and as three-layered sandwich with FGM core (skins with $h_1 = h_3 = 0.15h$ and core with $h_2 = 0.7h$). See Fig. 6 for further details about these two FGM configurations.

The one-layered FGM configuration (see Fig. 6) has the Young modulus and mass density defined in Eq. (40). The first material configuration is a one-layered functionally graded material structure where the bottom is fully metallic (m) (Aluminium Alloy Al2024: Young modulus $E_m = 73$ GPa, mass density $\rho_m = 2800$ kg/m^3 and Poisson ratio $\nu_m = 0.3$) and the top is fully ceramic (c) (Alumina Al_2O_3: Young modulus $E_c = 380$ GPa, mass density $\rho_c = 3800$ kg/m^3 and Poisson ratio $\nu_c = 0.3$). The Poisson ratio is constant through the thickness. Mass density and Young modulus vary through the thickness by means of the law indicated in Eqs. (40) where the volume fraction considered is that indicated in Eq. (42) for the ceramic phase ($V_c = 0$ at the bottom and $V_c = 1$ at the top). The exponents p used for the material law are p = 0.0, 0.5, 1.0, 2.0. $p = 0$ means fully ceramic structure. The volume fraction of the ceramic phase is defined by Eq. (42).

The second material configuration is the sandwich one (see Fig. 6). The bottom skin is metallic (Aluminum Alloy Al2024 as for the first configuration) and the top skin is a ceramic different from the Alumina Al_2O_3 used in the first configuration (Young modulus $E_c = 200$ GPa, mass density $\rho_c = 5700$ kg/m^3 and Poisson ratio $\nu_c = 0.3$). The functionally graded core has constant Poisson ratio. Mass density and Young modulus have the same variation already indicated for the first material configuration in Eqs. (40) and (42). The p exponents are 0.5, 1.0 and 2.0. A classical core is also considered with material properties which are an average between the top skin and the bottom skin ($E = \frac{E_c+E_m}{2}$, $\rho = \frac{\rho_c+\rho_m}{2}$ and Poisson ratio $\nu = 0.3$). For the FGM core the thickness used in Eq. (42) is $h_c = 0.7h$.

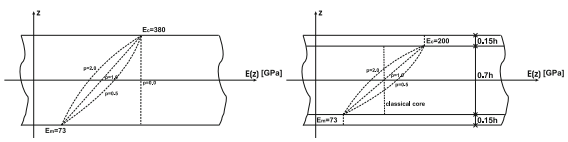

Fig. 6 Functionally graded material law through the thickness direction for the one-layered benchmarks (on the *left*) and sandwich benchmarks (on the *right*)

The 2D FE convergence study considers two examples: a simply supported one-layered FGM plate with p = 1 (see Fig. 7) and a sandwich cylinder with FGM core (p = 0.5) and classical skins (see Fig. 8). In the first example of Fig. 7 a good convergence of the 2D FE model with respect the 3D exact solution is obtained for a 69×69 mesh which means 4760 element. This mesh will be always used for all the plate results in Sect. 5. In the second example of Fig. 8 a good convergence of the 2D FE model with respect the 3D exact solution is obtained for a 127×38 mesh which means 4826 elements. This mesh will be always used for all the cylinder results in Sect. 5. This convergence study is valid for both thick and thin strcutures as clearly indicated in Figs. 7 and 8.

The 2D FE model has been validated for both geometries (plates and cylinders) and for different material configurations. The FE model correctly converges with a 69×69 mesh for the plate geometry, and with a 127×38 mesh for the cylinder. Such values will always be used in Sect. 5 for the detailed comparison between the 3D exact solution and the 2D numerical models.

4 Refined 2D generalized differential quadrature (GDQ) methods

In the present paper two refined 2D shell models have been considered in accordance with the unified formulation by Carrera proposed in [62]. An equivalent single layer model and a layer-wise approach are described. The first model considers the following displacement field

$$\mathbf{U} = \sum_{\tau=0}^{N_c+1} \mathbf{F}_\tau \mathbf{u}^{(\tau)}, \tag{43}$$

where $\mathbf{U}$ indicates the 3D displacement components and $\mathbf{u}$ stands for the vector of the τth generalized displacements of the points on the middle surface of

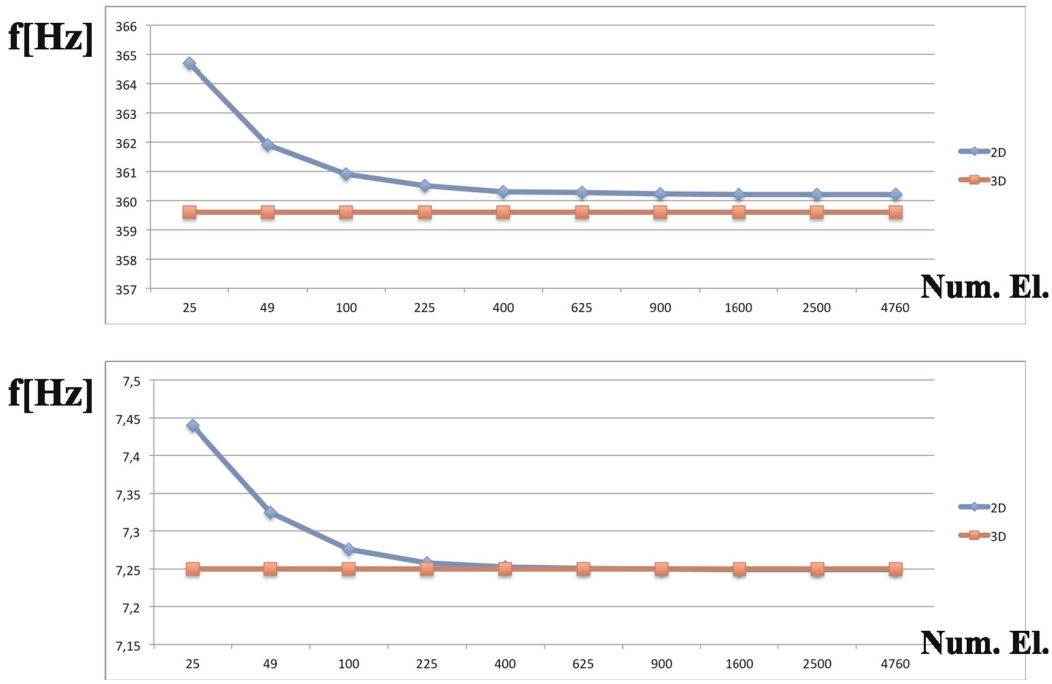

Fig. 7 Convergence analysis via 2D FE for the first frequency of the simply supported one-layered FGM plate with $p = 1.0$. $a/h = 20$ at the *top* and $a/h = 1000$ at the *bottom*

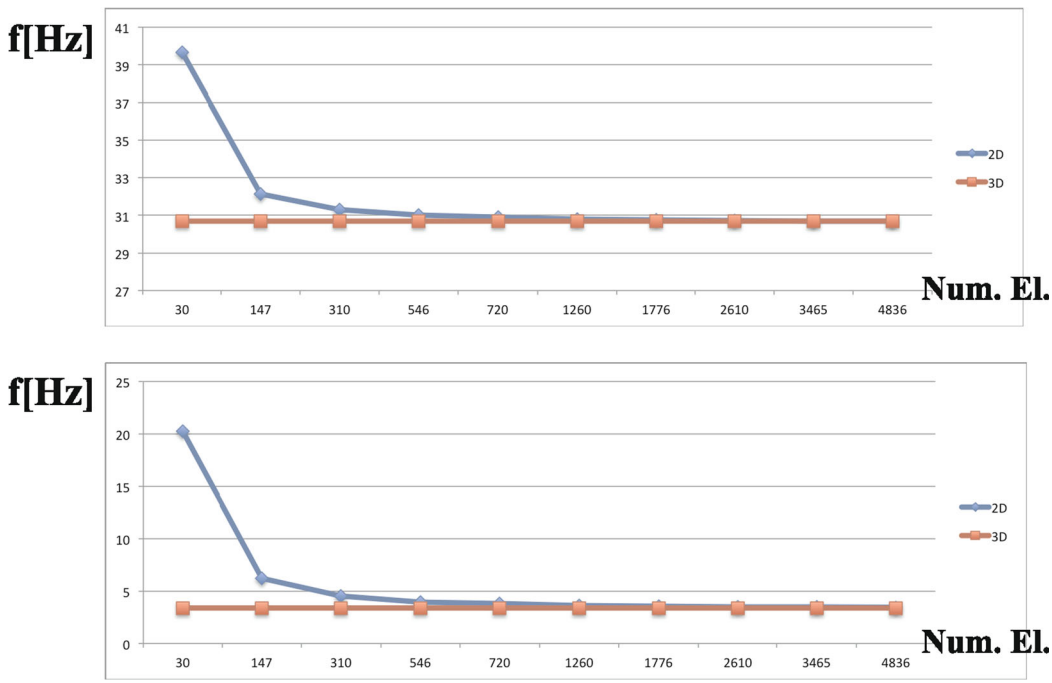

Fig. 8 Convergence analysis via 2D FE for the first frequency of the simply supported sandwich cylinder with FGM core ($p = 0.5$). $R_\alpha/h = 10$ at the *top* and $R_\alpha/h = 1000$ at the *bottom*

the shell [56]. $\mathbf{F}_{\tau(ij)} = \delta_{ij} F_\tau$, for $i,j = 1,2,3$ is the thickness function matrix and δ is the Kronecker delta function. Considering the present general higher-order approach, the classic first order model based on the Reissner–Mindlin hypotheses can be deducted when $\tau = 0, 1$ or $N_c = 0$ (GDQ-RM). A higher-order expansion with $N_c = 4$ means GDQ-ESL. When the zig-zag function is added for multilayered structures, a GDQ-ZZ model is defined. It is obvious that structures made of a single ply do not need a zigzag effect.

Due to the arbitrary expansion τ, the relation between generalized strains $\boldsymbol{\varepsilon}^{(\tau)}$ (defined for the generic order τ) and displacement parameters $\mathbf{u}^{(\tau)}$ can be reported, according to [56], as

$$\boldsymbol{\varepsilon}^{(\tau)} = \mathbf{D}_\Omega \mathbf{u}^{(\tau)} \quad \text{for} \quad \tau = 0,1,2,\ldots,N_c,N_c+1, \tag{44}$$

where the definition of $\mathbf{D}_\Omega$ can be found in explicit form in [56].

The τth order resultants in terms of generalized sth order strains $\boldsymbol{\varepsilon}^{(s)}$ can be defined as

$$\mathbf{S}^{(\tau)} = \sum_{s=0}^{N_c+1} \mathbf{A}^{(\tau s)} \boldsymbol{\varepsilon}^{(s)} \quad \text{for} \quad \tau = 0,1,2,\ldots,N_c,N_c+1 \tag{45}$$

where the elastic coefficients of the constitutive matrix $\mathbf{A}^{(\tau s)} = \sum_{k=1}^{N_L} \int_{z_k}^{z_{k+1}} \left(\mathbf{Z}^{(\tau)}\right)^T \bar{\mathbf{C}}^{(k)} \mathbf{Z}^{(s)} H_\alpha H_\beta dz$ are also reported in extended form in [56], where $\bar{\mathbf{C}}^{(k)}$ is the constitutive matrix for the kth ply and $\mathbf{Z}^{(\tau)}$ is a geometric matrix.

The current generalized approach has, for each τ order, three motion equations which are functions of the internal actions as in the following

$$\mathbf{D}_\Omega^\star \mathbf{S}^{(\tau)} = \sum_{s=0}^{N_c+1} \mathbf{M}^{(\tau s)} \ddot{\mathbf{u}}^{(s)} \quad \text{for} \quad \tau = 0,1,2,\ldots,N_c,N_c+1, \tag{46}$$

where $\mathbf{D}_\Omega^\star$ is the equilibrium operator and $\mathbf{M}^{(\tau s)}$ is the inertia matrix. They can be found in explicit form in [56]. In detail, the mass matrix $\mathbf{M}_{(ij)}^{(\tau s)} = \delta_{ij} I_0^{(\tau s)}$ contains the inertia mass terms $I_0^{(\tau s)}$ for $i,j = 1,2,3$ and can be evaluated as

$$I_0^{(\tau s)} = \sum_{k=1}^{N_L} \int_{z_k}^{z_{k+1}} \rho^{(k)} F_\tau F_s H_\alpha H_\beta dz \quad \text{for} \quad \tau, s = 0,1,2,\ldots,N_c,N_c+1, \tag{47}$$

where $\rho^{(k)}$ represents the mass density of the material per unit of volume of the kth ply. Combining the kinematic (44), constitutive (45) and motion (46) equations, the fundamental system of equations in terms of displacement parameters can be found

$$\sum_{s=0}^{N_c+1} \mathbf{L}^{(\tau s)} \mathbf{u}^{(s)} = \sum_{s=0}^{N_c+1} \mathbf{M}^{(\tau s)} \ddot{\mathbf{u}}^{(s)} \quad \text{for} \quad \tau = 0,1,2,\ldots,N_c,N_c+1, \tag{48}$$

where $\mathbf{L}^{(\tau s)} = \mathbf{D}_\Omega^\star \mathbf{A}^{(\tau s)} \mathbf{D}_\Omega$ is the fundamental operator [56].

Boundary conditions must be introduced to solve the differential problem in Eq.(48). Combining conveniently the kinematic and static conditions, any boundary condition can be enforced. Generally, three configurations are the most classic ones [56]: clamped edge boundary conditions (C), free edge boundary conditions (F) and simply-supported edge boundary conditions (S). Only simply-supported structures are investigated in this paper in order to make the comparisons with the three-dimensional exact results:

$$\begin{aligned}
&N_\alpha^{(\tau)} = 0,\ u_\beta^{(\tau)} = u_z^{(\tau)} = 0 \\
&\tau = 0,1,2,\ldots,N_c,N_c+1 \quad \text{at} \quad \alpha = \alpha^0 \quad \text{or} \\
&\alpha = \alpha^1 \quad \beta^0 \le \beta \le \beta^1, \\
&u_\alpha^{(\tau)} = 0,\ N_\beta^{(\tau)} = 0,\ u_z^{(\tau)} = 0 \\
&\tau = 0,1,2,\ldots,N_c,N_c+1 \quad \text{at} \quad \beta = \beta^0 \quad \text{or} \\
&\beta = \beta^1 \quad \alpha^0 \le \alpha \le \alpha^1.
\end{aligned} \tag{49}$$

When higher-order generalized layer-wise models are taken into account (GDQ-LW), the mathematical background follows similar guidelines provided by the equivalent single layer model. In fact, the displacement field takes the following form [60]

$$\mathbf{U}^{(k)} = \sum_{\tau=0}^{N_c+1} \mathbf{F}_\tau^{(k)} \mathbf{u}^{(k\tau)} \quad \text{for} \quad k = 1,2,\ldots,N_L. \tag{50}$$

Comparing Eq.(50) with Eq.(43) it is noted that each quantity is referred to each single layer (k). The thickness functions are assumed in the classic manner [60] as

$$F_{\tau}^{(k)} = \begin{cases} \dfrac{Q_0 - Q_1}{2} = \dfrac{1-\bar{z}_k}{2} & \text{for} \quad \tau = 0 \\ Q_{\tau+1} - Q_{\tau-1} & \text{for} \quad \tau = 1,2,\ldots,N_c \\ \dfrac{Q_0 + Q_1}{2} = \dfrac{1+\bar{z}_k}{2} & \text{for} \quad \tau = N_c+1 \end{cases} \tag{51}$$

where Q_τ are the Legendre polynomials recursively defined in [60], and $\bar{z}_k$ is the dimensionless thickness co-ordinate $\bar{z}_k(z) = z_k(z^{(k)}) \in [-1,1]$. Considering the kth layer it becomes $z_k = 2z^{(k)}/h_k$. The generalized displacements $u_\alpha^{(k0)}$, $u_\beta^{(k0)}$, $u_z^{(k0)}$ for $\tau = 0$ are the displacements at the bottom of the kth layer $(z^{(k)} = -h_k/2)$, whereas $u_\alpha^{(k(N_c+1))}$, $u_\beta^{(k(N_c+1))}$, $u_z^{(k(N_c+1))}$ for $\tau = N_c+1$ are the displacements at the top of the kth layer $(z^{(k)} = +h_k/2)$.

Due to the present displacement field of Eq. (50), the kinematic equations can be found:

$$\boldsymbol{\varepsilon}^{(k\tau)} = \mathbf{D}_\Omega^{(k)} \mathbf{u}^{(k\tau)} \quad \text{for} \quad \tau = 0,1,2,\ldots,N_c,N_c+1, \quad k = 1,2,\ldots,N_L, \tag{52}$$

where $\mathbf{D}_\Omega^{(k)}$ have been explicitly reported in [60]. Since a linear and elastic material has been considered, the relationships between stresses and strains for the kth ply follow the Hooke's law, as reported extensively in [60], and the internal actions, layer by layer, take the final form

$$\mathbf{S}^{(k\tau)} = \sum_{s=0}^{N_c+1} \mathbf{A}^{(k\tau s)} \boldsymbol{\varepsilon}^{(ks)} \quad \text{for} \quad \tau = 0,1,2,\ldots,N_c,N_c+1, \quad k = 1,2,\ldots,N_L, \tag{53}$$

where $\mathbf{A}^{(k\tau s)} = \sum_{k=1}^{N_L} \int_{-h_k/2}^{+h_k/2} \left(\mathbf{Z}^{(k\tau)}\right)^T \bar{\mathbf{C}}^{(k)} \mathbf{Z}^{(ks)} H_\alpha^{(k)} H_\beta^{(k)} dz^{(k)}$ and where the matrices $\mathbf{Z}^{(k\tau)}$ and $\mathbf{Z}^{(ks)}$ have been presented in [60]. The τth order generalized internal action is indicated as $\mathbf{S}^{(k\tau)}$ and the elastic coefficients are $\mathbf{A}^{(k\tau s)}$ which have been already presented in [60].

The equation of motion are deducted from the Hamilton's Principle, in particular a set of three equilibrium equations for each order τ can be found

$$\mathbf{D}_\Omega^{\star(k)} \mathbf{S}^{(k\tau)} = \sum_{s=0}^{N_c+1} \mathbf{M}^{(k\tau s)} \ddot{\mathbf{u}}^{(ks)} \quad \text{for} \quad \tau = 0,1,2,\ldots,N_c,N_c+1, \quad k = 1,2,\ldots,N_L, \tag{54}$$

where the equilibrium operator $\mathbf{D}_\Omega^{\star(k)} \mathbf{S}^{(k\tau)}$ and the inertia matrix $\mathbf{M}^{(k\tau s)}$ have been explicitly shown in [60].

Finally the fundamental equations in terms of generalized displacements take the form

$$\sum_{s=0}^{N_c+1} \mathbf{L}^{(k\tau s)} \mathbf{u}^{(ks)} = \sum_{s=0}^{N_c+1} \mathbf{M}^{(k\tau s)} \ddot{\mathbf{u}}^{(ks)} \quad \text{for} \quad \tau = 0,1,2,\ldots,N_c,N_c+1, \quad k = 1,2,\ldots,N_L, \tag{55}$$

where $\mathbf{L}^{(k\tau s)} = \mathbf{D}_\Omega^{\star(k)} \mathbf{A}^{(k\tau s)} \mathbf{D}_\Omega^{(k)}$ [60] is the fundamental operator. Since the approach is based on a layer-by-layer structure, the compatibility conditions between the layers must be defined. In detail, the top displacements of the kth ply at each interface must be equal to the bottom displacements of the $(k+1)$th layer, as

$$\begin{bmatrix} u_\alpha^{(k\,\mathrm{top})} \\ u_\beta^{(k\,\mathrm{top})} \\ u_z^{(k\,\mathrm{top})} \end{bmatrix} = \begin{bmatrix} u_\alpha^{((k+1)\mathrm{bottom})} \\ u_\beta^{((k+1)\mathrm{bottom})} \\ u_z^{((k+1)\mathrm{bottom})} \end{bmatrix} \rightarrow \begin{bmatrix} u_\alpha^{(k(N_c+1))} \\ u_\beta^{(k(N_c+1))} \\ u_z^{(k(N_c+1))} \end{bmatrix} = \begin{bmatrix} u_\alpha^{((k+1)0)} \\ u_\beta^{((k+1)0)} \\ u_z^{((k+1)0)} \end{bmatrix} \quad \text{for} \quad \begin{matrix} \tau = 0,1,2,\ldots,N_c,N_c+1 \\ k = 1,2,\ldots,N_L-1 \end{matrix} \tag{56}$$

In conclusion, three types of boundary conditions can be reported, by means of the GDQ method, which have to be enforced for solving the partial differential system of equations [60]: clamped edge boundary conditions (C), free edge boundary conditions (F) and simply-supported edge boundary conditions (S). Only simply-supported structures are investigated in this paper in order to make the comparisons with the three-dimensional exact results:

$$\begin{aligned} N_{\alpha}^{(k\tau)} = 0, u_{\beta}^{(k\tau)} = u_{z}^{(k\tau)} = 0 \quad \text{for} \quad \begin{matrix} \tau = 0, 1, 2, \ldots, N_c, N_c + 1 \\ k = 1, 2, \ldots, N_L \end{matrix} \quad \text{at} \quad \begin{matrix} \alpha = \alpha^0 \quad \text{or} \quad \alpha = \alpha^1 \\ \beta^0 \leq \beta \leq \beta^1 \end{matrix} \\ u_{\alpha}^{(k\tau)} = 0, N_{\beta}^{(k\tau)} = 0, u_{z}^{(k\tau)} = 0 \quad \text{for} \quad \begin{matrix} \tau = 0, 1, 2, \ldots, N_c, N_c + 1 \\ k = 1, 2, \ldots, N_L \end{matrix} \quad \text{at} \quad \begin{matrix} \beta = \beta^0 \quad \text{or} \quad \beta = \beta^1 \\ \alpha^0 \leq \alpha \leq \alpha^1 \end{matrix} \end{aligned} \tag{57}$$

4.1 Validation of the refined GDQ models

The stability and accuracy of the GDQ method has been proven in several applications already published in the literature [49–60]. Generally the GDQ method needs a very small amount of points in order to find an accurate solution. In fact, for flat structures, such as plates, the solution is accurate when the number of points is small [49–60]. The number of points are functions of the geometry of the problem under investigation. A cylindrical shell made of a single ply of Alumina with $R_\alpha/h = 1000$ is considered in Fig. 9, the first ten non-symmetric mode shapes represent the first twenty natural frequencies of the structure. It can be observed from Fig. 9, where GDQ-RM and GDQ-LW are used, that low order modes can be captured using few points, however higher-order modes need at least 51 points along the circular cross-section of the cylinder to have a stable solution and capture all the circumferential modes. On the contrary on the meridian direction fewer points are kept to describe meridian mode waves. In fact, the figures report the first nineteen frequencies of cylindrical shells using $I_N \times 15$ points with $I_N = 15, 17, \ldots, 51$. In all the computations made in this paper, a Chebyshev–Gauss–Lobatto grid has been considered [42], so that the points along the α and β directions are not distributed uniformly but they follow a cosine function. In conclusion, for the flat plate computations a 25×25 grid has been considered (see [49–60]), whereas for the cylindrical shells a 51×15 grid is used (see Fig. 9).

5 Results

This section proposes a detailed comparison between the 3D exact model validated and discussed in Sect. 2, the 2D FE model obtained via the code MSC Nastran & Patran [48] validated and discussed in Sect. 3, and classical and refined GDQ models discussed and validated in Sect. 4. The 3D exact results use an order of expansion $N = 3$ for the exponential matrix, and $p = 100$ fictitious layers for shell and FGM description. The 2D FE results use the SHELL QUAD4 element of Nastran with a 69×69 mesh for all the plate geometries and a 127×38 mesh for all the cylinder geometries. In this case $p = 100$ fictitious layer are also used for the FGM description. The classical and refined 2D GDQ models use a 25×25 Chebyshev–Gauss–Lobatto grid for the flat plates and a 51×15 Chebyshev–Gauss–Lobatto grid for the cylindrical shells. The comparisons will be made only for plates and cylinders in order to focus our attention to several laminations and materials. In this way, we are able to contain the length of the paper and we do not lose in clarity. For cylindrical geometries, frequencies with $w \neq 0$ are obtained twice by Nastran (for each couple of (m, n)) because the section of the cylinder is symmetric. However, these two vibration modes are equal and we will write only one frequency in the tables. Further geometries, such as cylindrical and spherical shell panels, could be the topic of a future comparison work.

5.1 Comparison between the three models

Four different benchmarks will be analyzed in this section to compare these three different methods (see Fig. 3c, d). The first benchmark is a one-layered FGM simply supported plate with different thickness ratios a/h (several p coefficients will be considered in the FGM law). The second benchmark is a sandwich plate with two external classical skins and an internal FGM core, and different thickness ratios a/h. The core could be in FGM with different p coefficients or classical. The third benchmark is a one-layered FGM cylinder with different thickness ratios R_α/h (the same FGM

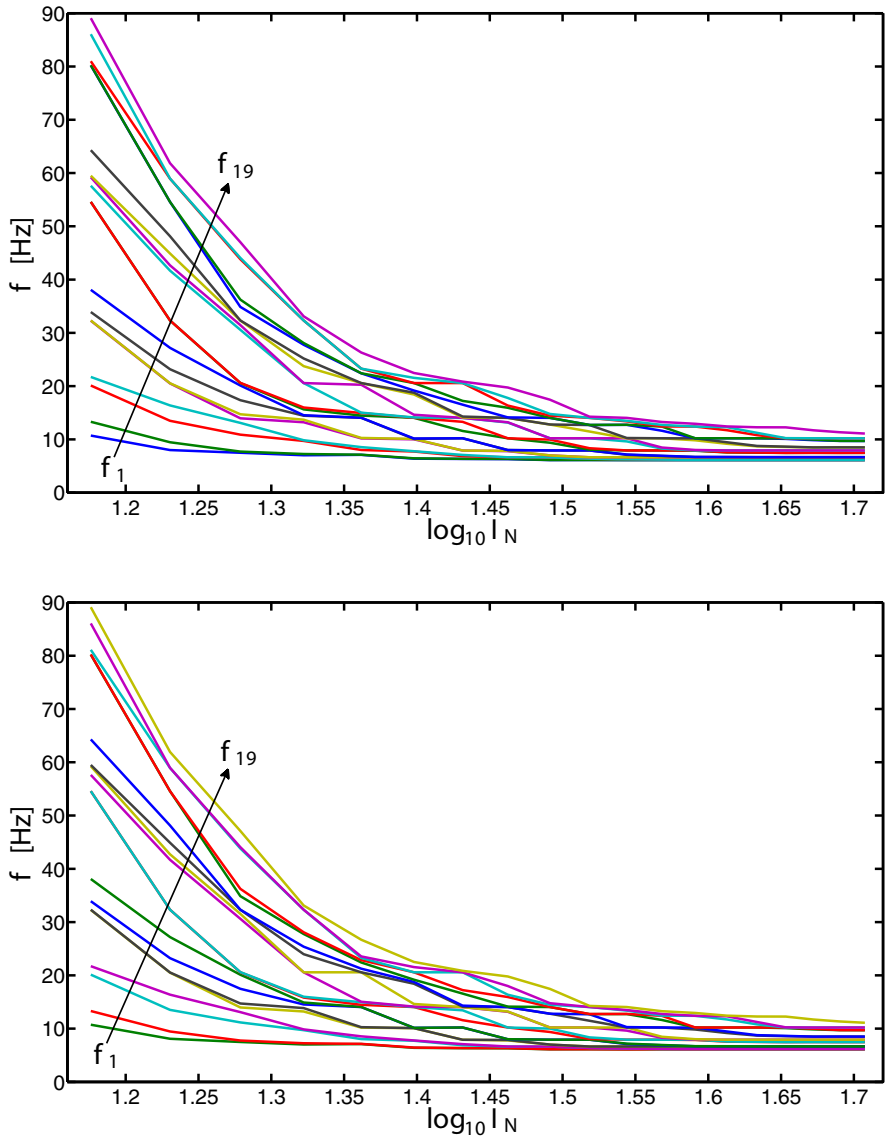

Fig. 9 Convergence of the first nineteen natural frequencies of a simply-supported cylinder made of a single ply of Alumina varying the number of point in the circumferential direction ($I_N \times 15$) using a linear model GDQ-RM (at the *top*) and a higher-order layer-wise model GDQ-LW (at the *bottom*)

law already seen for the first benchmark). The fourth benchmark is a sandwich cylinder with different thickness ratios R_α/h (the two skins and the internal core have the same characteristics already seen for the second benchmark). All the details about these four different benchmarks have already been given in Sect. 3 where the 2D FE model has been validated.

For all the benchmarks, the comparison is proposed calculating the first ten frequencies via the 2D FE code. From the visualization of these ten vibrations modes, it is possible to understand the half-wave numbers m and n in the α and β directions. Therefore, these half-wave numbers have been used to calculate the same ten frequencies via the 3D exact model. For each couple of m and n, the 3D exact model gives infinite frequencies (from I, II, III until ∞). In the tables, in-plane modes are indicated with $w = 0$. There are some frequencies missed by the FE code, but they have not been investigated via the 3D exact model because this is not the main aim of the paper. The main aim of the paper is to understand the differences between the 2D numerical models and the 3D exact model for the first ten frequencies given by the 2D FE code. The classical and refined 2D GDQ models do not need to a priori know the half-wave numbers because they are numerical methods. It is also important to

understand what are the features that influence the differences between the several models proposed in this paper (geometry of the structures, materials, lamination sequences, thickness ratios, order of frequencies, vibration modes).

Tables 3, 4, 5, and 6 show frequency results for the one-layered FGM plate. The FGM law uses parameters p equal 0.0, 0.5, 1.0 and 2.0. In each table thick and thin plates are investigated (thickness ratios a/h from 10 to 1000). The benchmark proposed in Table 3 is a classical ceramic plate ($p = 0.0$), in this case for thick structures the differences between the 3D exact model and the 2D FE model are very important. Such differences are similar for the comparison between the 3D exact model and the GDQ-RM approach which makes use of the same kinematic model of the 2D FE model (Reissner–Mindlin theory). Refined ESL and LW GDQ models give results very similar to the exact 3D model because they are refined 2D models with higher order of expansion for the displacement components through the thickness direction. The plate is one-layered with an isotropic ceramic material ($p = 0.0$). For this reason, in the case of thin structures (a/h equals 100 or 100), the results obtained by means of exact, GDQ and FE models are very similar. For thick plates, in the first ten frequencies there are some in-plane modes (transverse displacement $w = 0$). In this case, the 2D FE model gives correct results even if a Reissner–Mindlin model is used because the kinematic hypotheses of this model are correct for this mode case. Similar considerations can be made for Tables 4, 5 and 6 where the plate is made of a functionally graded material with parameter p equals 0.5, 1.0 and 2.0, respectively. Refined ESL and LW GDQ models are mandatory to obtain correct values for both low and higher order modes and for both thick and thin structures. The 2D FE model gives some problems for higher order frequencies and/or thick plates. Figure 10 is an example of the first five vibration modes obtained via the 2D FE model, a thick plate ($a/h = 10$) and an FGM law with $p = 1.0$ are considered. The 2D FE modes are in the left column and the exact 3D vibration modes are in the right column. The FE vibration modes are plotted for all the three directions (α, β, z), they allow to understand the half-wave numbers m and n to use for the exact 3D results. In this last case, the vibration modes in the in-plane directions are known by means of m and n values. Therefore, only the non-dimensional displacement amplitudes $u^* = U/U_{max}$, $v^* = V/V_{max}$ and $w^* = W/W_{max}$ trough the non-dimensional thickness coordinate $z^* = z/h$ are given. From both 2D FE and 3D exact vibration modes is clear how the fourth and fifth frequencies are in-plane vibration modes with zero transverse displacement w.

Tables 7, 8, 9 and 10 propose the first ten frequencies obtained by means of the 2D FE model in the case of a sandwich plate with FGM core and external classical skins. Table 7 considers a classical core where the elastic properties are an average between the properties of the ceramic skin and the metallic skin. Tables 8, 9 and 10 considers FGM core with exponential parameter p equals 0.5, 1.0 and 2.0, respectively. Considerations similar to the one-layered case (Tables 3, 4, 5, 6) can be obtained. The 2D FE model gives correct results only for thin structures and low frequencies. 3D exact results are correctly obtained for both thin and thick plates and for low and high frequencies only if 2D refined models are used (see the frequencies obtained by means the refined 2D ZZ and LW models solved via the GDQ method). In the case of multilayered structures, a zigzag Murakami function is included in the refined ESL model in order to recovery the typical zigzag form of the displacements due to the transverse anisotropy. 2D FE model gives correct results for in-plane modes (even if thick plates and higher frequencies are considered) because the transverse displacement w is zero and the Reissner–Mindlin model correctly describes the kinematic of this analyzed mode. Both 2D FE model and GDQ-RM model have several problems for thick plates and/or higher frequencies because they use a simplified kinematic model such as the Reissner–Mindlin one. In this cases the use of refined 2D models (GDQ-ZZ and GDQ-LW) is mandatory to obtain the 3D exact results.

Tables 11, 12, 13 and 14 give the frequency and vibration mode analysis in the case of one-layered FGM cylinders. The FGM layer has the same properties already seen for the one-layered plate case. The first column of each table includes the first ten frequencies obtained via the 2D FE model. For each frequency, the vibration modes are plotted in order to understand the half-wave numbers m and n to use for the 3D exact analysis. For cylinders, the circumferential half wave numbers m can have only even values because the cylinder has a closed geometry in the α-direction. m and n values are used to calculate the 3D exact results. GDQ results are numerical methods and they do not need to know a priori the half-wave

Table 3 First benchmark, simply supported one-layered FGM plate with p = 0.0 and several thickness ratios a/h. First ten frequencies in Hz for the present 3D exact solution and several numerical solutions

$p = 0.0$						
2D FE	m, n	Mode	3D exact	GDQ-RM	GDQ-ESL	GDQ-LW
$a/h = 10$						
925.0	1, 1	I	919.4	918.2	919.4	919.4
2226	2, 1	I	2197	2191	2197	2197
2226	1, 2	I	2197	2191	2197	2197
3101	0, 1	II($w = 0$)	3101	3101	3101	3101
3101	1, 0	II($w = 0$)	3101	3101	3101	3101
3436	2, 2	I	3376	3361	3376	3376
4203	3, 1	I	4117	4096	4117	4117
4203	1, 3	I	4117	4096	4117	4117
4386	1, 1	II($w = 0$)	4385	4385	4385	4385
5289	3, 2	I	5171	5138	5171	5171
$a/h = 20$						
472.0	1, 1	I	471.3	471.1	471.3	471.3
1168	2, 1	I	1163	1162	1163	1163
1168	1, 2	I	1163	1162	1163	1163
1850	2, 2	I	1839	1836	1839	1839
2300	3, 1	I	2280	2277	2280	2280
2300	1, 3	I	2280	2277	2280	2280
2959	3, 2	I	2931	2925	2931	2931
2959	2, 3	I	2931	2925	2931	2931
3101	1, 0	II($w = 0$)	3101	3101	3101	3101
3101	0, 1	II($w = 0$)	3101	3101	3101	3101
$a/h = 100$						
95.05	1, 1	I	95.03	95.03	95.04	95.04
237.6	2, 1	I	237.5	237.5	237.5	237.5
237.6	1, 2	I	237.5	237.5	237.5	237.5
379.9	2, 2	I	379.7	379.7	379.7	379.7
475.2	3, 1	I	474.5	474.5	474.5	474.5
475.2	1, 3	I	474.5	474.5	474.5	474.5
617.2	3, 2	I	616.5	616.5	616.5	616.5
617.2	2, 3	I	616.5	616.5	616.5	616.5
808.1	4, 1	I	805.7	805.6	805.7	805.7
808.1	1, 4	I	805.7	805.6	805.7	805.7
$a/h = 1000$						
9.500	1, 1	I	9.500	9.507	9.507	9.507
23.78	2, 1	I	23.76	23.77	23.77	23.77
23.78	1, 2	I	23.76	23.77	23.77	23.77
38.03	2, 2	I	38.02	38.03	38.03	38.03
47.59	1, 3	I	47.53	47.53	47.53	47.53
47.59	3, 1	I	47.53	47.53	47.53	47.53
61.83	2, 3	I	61.79	61.79	61.79	61.79
61.83	3, 2	I	61.79	61.79	61.79	61.79
81.00	4, 1	I	80.80	80.81	80.81	80.81
81.00	1, 4	I	80.80	80.81	80.81	80.81

Table 4 First benchmark, simply supported one-layered FGM plate with p = 0.5 and several thickness ratios a/h. First ten frequencies in Hz for the present 3D exact solution and several numerical solutions

p = 0.5						
2D FE	m, n	Mode	3D exact	GDQ-RM	GDQ-ESL	GDQ-LW
$a/h = 10$						
784.0	1, 1	I	778.0	778.5	779.9	779.9
1894	1, 2	I	1871	1863	1871	1871
1894	2, 1	I	1871	1863	1871	1871
2774	1, 0	II($w = 0$)	2775	2775	2775	2775
2774	0, 1	II($w = 0$)	2775	2775	2775	2775
2932	2, 2	I	2885	2867	2884	2884
3594	1, 3	I	3525	3499	3524	3524
3594	3, 1	I	3525	3499	3524	3524
3922	1, 1	II($w = 0$)	3923	3923	3923	3923
4535	2, 3	I	4438	4399	4437	4437
$a/h = 20$						
399.3	1, 1	I	398.9	398.6	398.8	398.8
989.3	2, 1	I	985.9	984.6	985.7	985.7
989.3	1, 2	I	985.8	984.6	985.7	985.7
1568	2, 2	I	1560	1557	1560	1560
1950	3, 1	I	1936	1931	1936	1936
1950	1, 3	I	1936	1931	1936	1936
2512	3, 2	I	2490	2483	2490	2490
2512	2, 3	I	2490	2483	2490	2490
2775	1, 0	II($w = 0$)	2775	2775	2775	2775
2775	0, 1	II($w = 0$)	2775	2775	2775	2775
$a/h = 100$						
80.34	1, 1	I	80.37	80.36	80.36	80.36
200.8	1, 2	I	200.8	200.8	200.8	200.8
200.8	2, 1	I	200.8	200.8	200.8	200.8
321.2	2, 2	I	321.2	321.1	321.1	321.1
401.7	3, 1	I	401.4	401.3	401.3	401.3
401.7	1, 3	I	401.4	401.3	401.3	401.3
521.7	3, 2	I	521.5	521.4	521.5	521.5
521.7	2, 3	I	521.5	521.4	521.5	521.5
683.2	4, 1	I	681.6	681.4	681.5	681.5
683.2	1, 4	I	681.6	681.4	681.5	681.5
$a/h = 1000$						
8.036	1, 1	I	8.040	8.039	8.039	8.039
20.10	2, 1	I	20.10	20.10	20.10	20.10
20.10	1, 2	I	20.10	20.10	20.10	20.10
32.15	2, 2	I	32.16	32.15	32.15	32.15
40.23	3, 1	I	40.20	40.19	40.19	40.19
40.23	1, 3	I	40.20	40.19	40.19	40.19
52.26	3, 2	I	52.26	52.25	52.25	52.25
52.26	2, 3	I	52.26	52.25	52.25	52.25
68.46	1, 4	I	68.34	68.33	68.33	68.33
68.46	4, 1	I	68.34	68.33	68.33	68.33

Table 5 First benchmark, simply supported one-layered FGM plate with p = 1.0 and several thickness ratios a/h. First ten frequencies in Hz for the present 3D exact solution and several numerical solutions

p = 1.0						
2D FE	m, n	Mode	3D exact	GDQ-RM	GDQ-ESL	GDQ-LW
$a/h = 10$						
707.3	1, 1	I	703.5	702.4	703.5	703.5
1709	2, 1	I	1689	1683	1689	1689
1709	1, 2	I	1689	1683	1689	1689
2567	1, 0	II($w = 0$)	2568	2568	2568	2568
2567	0, 1	II($w = 0$)	2568	2568	2568	2568
2647	2, 2	I	2605	2591	2605	2605
3245	3, 1	I	3184	3164	3184	3184
3245	1, 3	I	3184	3164	3184	3184
3628	1, 1	II($w = 0$)	3630	3630	3630	3630
4095	2, 3	I	4012	3980	4012	4012
$a/h = 20$						
360.2	1, 1	I	359.6	359.5	359.6	359.6
892.5	2, 1	I	889.0	888.1	889.0	889.0
892.5	1, 2	I	889.0	888.1	889.0	889.0
1415	2, 2	I	1407	1405	1407	1407
1760	3, 1	I	1746	1743	1746	1746
1760	1, 3	I	1746	1743	1746	1746
2266	2, 3	I	2247	2241	2247	2247
2266	3, 2	I	2247	2241	2247	2247
2569	1, 0	II($w = 0$)	2569	2569	2569	2569
2569	0, 1	II($w = 0$)	2569	2569	2569	2569
$a/h = 100$						
72.47	1, 1	I	72.46	72.46	72.46	72.46
181.2	1, 2	I	181.1	181.1	181.1	181.1
181.2	2, 1	I	181.1	181.1	181.1	181.1
289.7	2, 2	I	289.6	289.6	289.6	289.6
362.4	1, 3	I	361.9	361.8	361.8	361.8
362.4	3, 1	I	361.9	361.8	361.8	361.8
470.6	3, 2	I	470.2	470.1	470.2	470.2
470.6	2, 3	I	470.2	470.1	470.2	470.2
616.3	1, 4	I	614.5	614.4	614.5	614.5
616.3	4, 1	I	614.5	614.4	614.5	614.5
$a/h = 1000$						
7.249	1, 1	I	7.248	7.248	7.248	7.248
18.13	2, 1	I	18.12	18.12	18.12	18.12
18.13	1, 2	I	18.12	18.12	18.12	18.12
29.00	2, 2	I	29.00	28.99	28.99	28.99
36.29	3, 1	I	36.24	36.24	36.24	36.24
36.29	1, 3	I	36.24	36.24	36.24	36.24
47.14	3, 2	I	47.11	47.11	47.11	47.11
47.14	2, 3	I	47.11	47.11	47.11	47.11
61.76	4, 1	I	61.61	61.61	61.61	61.61
61.76	1, 4	I	61.61	61.61	61.61	61.61

Table 6 First benchmark, simply supported one-layered FGM plate with p = 2.0 and several thickness ratios a/h. First ten frequencies in Hz for the present 3D exact solution and several numerical solutions

p = 2.0						
2D FE	m, n	Mode	3D exact	GDQ-RM	GDQ-ESL	GDQ-LW
$a/h = 10$						
642.1	1, 1	I	638.8	638.9	638.8	638.8
1545	1, 2	I	1528	1528	1528	1528
1545	2, 1	I	1528	1528	1528	1528
2317	1, 0	II($w = 0$)	2317	2318	2317	2317
2317	0, 1	II($w = 0$)	2317	2318	2317	2317
2386	2, 2	I	2351	2351	2352	2352
2919	3, 1	I	2869	2869	2871	2871
2919	1, 3	I	2869	2869	2871	2871
3272	1, 1	II($w = 0$)	3274	3275	3274	3274
3676	3, 2	I	3603	3606	3610	3610
$a/h = 20$						
327.7	1, 1	I	327.2	327.2	327.2	327.2
811.1	2, 1	I	808.0	808.1	808.0	808.0
811.1	1, 2	I	808.0	808.1	808.0	808.0
1284	2, 2	I	1278	1278	1278	1278
1596	3, 1	I	1585	1585	1585	1585
1596	1, 3	I	1585	1585	1585	1585
2054	3, 2	I	2037	2037	2037	2037
2054	2, 3	I	2037	2037	2037	2037
2319	1, 0	II($w = 0$)	2319	2319	2319	2319
2319	0, 1	II($w = 0$)	2319	2319	2319	2319
$a/h = 100$						
65.98	1, 1	I	65.97	65.98	65.98	65.98
164.9	1, 2	I	164.9	164.9	164.9	164.9
164.9	2, 1	I	164.9	164.9	164.9	164.9
263.7	2, 2	I	263.6	263.6	263.6	263.6
329.9	3, 1	I	329.4	329.4	329.4	329.4
329.9	1, 3	I	329.4	329.4	329.4	329.4
428.4	3, 2	I	428.0	428.0	428.0	428.0
428.4	2, 3	I	428.0	428.0	428.0	428.0
561.0	4, 1	I	559.4	559.4	559.4	559.4
561.0	1, 4	I	559.4	559.4	559.4	559.4
$a/h = 1000$						
6.600	1, 1	I	6.590	6.600	6.600	6.600
16.50	1, 2	I	16.50	16.50	16.50	16.50
16.50	2, 1	I	16.50	16.50	16.50	16.50
26.40	2, 2	I	26.39	26.40	26.40	26.40
33.04	3, 1	I	32.99	33.00	33.00	33.00
33.04	1, 3	I	32.99	33.00	33.00	33.00
42.92	3, 2	I	42.89	42.90	42.90	42.90
42.92	2, 3	I	42.89	42.90	42.90	42.90
56.23	4, 1	I	56.09	56.10	56.10	56.10
56.23	1, 4	I	56.09	56.10	56.10	56.10

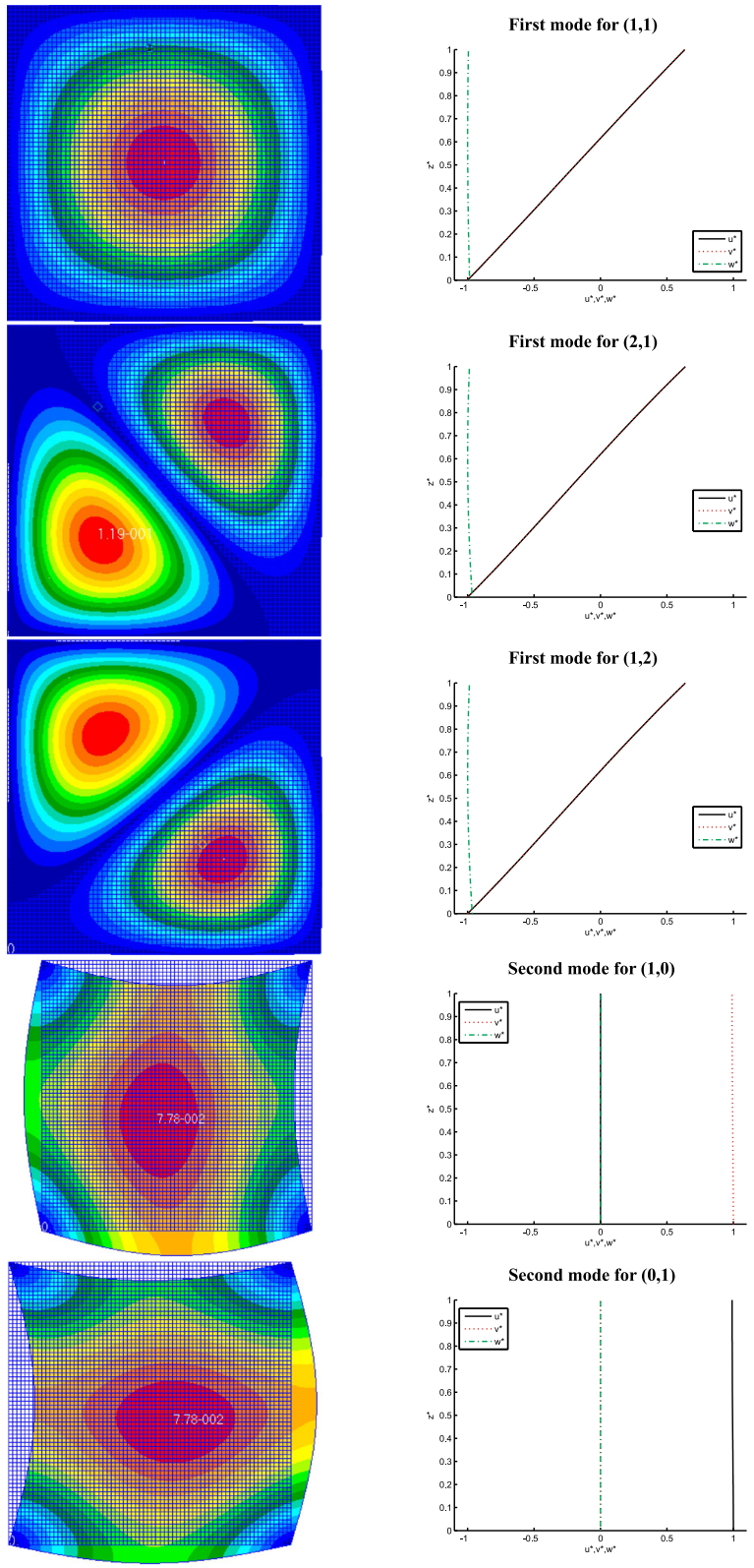

Fig. 10 First benchmark, simply supported FGM plate with $p = 1.0$ and thickness ratio $a/h = 10$. First five frequencies via 2D FE solution (on the *left*) and via 3D exact solution (on the *right*)

Table 7 Second benchmark, simply supported sandwich plate with classical core and several thickness ratios a/h. First ten frequencies in Hz for the present 3D exact solution and several numerical solutions

Classical core						
2D FE	m, n	Mode	3D exact	GDQ-RM	GDQ-ZZ	GDQ-LW
$a/h = 10$						
513.2	1, 1	I	510.3	509.9	510.4	510.3
1236	1, 2	I	1221	1218	1221	1221
1236	2, 1	I	1221	1218	1221	1221
1757	0, 1	II($w = 0$)	1757	1757	1757	1757
1757	1, 0	II($w = 0$)	1757	1757	1757	1757
1908	2, 2	I	1877	1872	1878	1877
2334	3, 1	I	2290	2282	2291	2290
2334	1, 3	I	2290	2282	2291	2290
2485	1, 1	II($w = 0$)	2485	2485	2485	2485
2939	3, 2	I	2878	2866	2879	2878
$a/h = 20$						
261.8	1, 1	I	261.4	261.4	261.4	261.4
648.2	1, 2	I	645.6	645.2	645.6	645.6
648.2	2, 1	I	645.6	645.2	645.6	645.6
1027	2, 2	I	1021	1020	1021	1021
1276	1, 3	I	1266	1265	1266	1266
1276	3, 1	I	1266	1265	1266	1266
1642	3, 2	I	1627	1625	1628	1627
1642	2, 3	I	1627	1625	1628	1627
1757	1, 0	II($w = 0$)	1757	1757	1757	1757
1757	0, 1	II($w = 0$)	1757	1757	1757	1757
$a/h = 100$						
52.72	1, 1	I	52.71	52.71	52.71	52.71
131.8	1, 2	I	131.7	131.7	131.7	131.7
131.8	2, 1	I	131.7	131.7	131.7	131.7
210.7	2, 2	I	210.6	210.6	210.6	210.6
263.6	1, 3	I	263.2	263.2	263.2	263.2
263.6	3, 1	I	263.2	263.2	263.2	263.2
342.3	3, 2	I	342.0	342.0	342.0	342.0
342.3	2, 3	I	342.0	342.0	342.0	342.0
448.2	1, 4	I	446.9	446.9	446.9	446.9
448.2	4, 1	I	446.9	446.9	446.9	446.9
$a/h = 1000$						
5.273	1, 1	I	5.272	5.273	5.273	5.273
13.19	2, 1	I	13.18	13.18	13.18	13.18
13.19	1, 2	I	13.18	13.18	13.18	13.18
21.10	2, 2	I	21.09	21.09	21.09	21.09
26.40	3, 1	I	26.36	26.36	26.36	26.36
26.40	1, 3	I	26.36	26.36	26.36	26.36
34.29	3, 2	I	34.27	34.27	34.27	34.27
34.29	2, 3	I	34.27	34.27	34.27	34.27
44.92	4, 1	I	44.82	44.82	44.82	44.82
44.92	1, 4	I	44.82	44.82	44.82	44.82

Table 8 Second benchmark, simply supported sandwich plate with FGM core (p = 0.5) and several thickness ratios a/h. First ten frequencies in Hz for the present 3D exact solution and several numerical solutions

FGM core with p = 0.5						
2D FE	m, n	Mode	3D exact	GDQ-RM	GDQ-ZZ	GDQ-LW
$a/h = 10$						
494.6	1, 1	I	492.1	491.2	492.1	492.1
1196	1, 2	I	1183	1178	1183	1183
1196	2, 1	I	1183	1178	1183	1183
1780	0, 1	II($w = 0$)	1781	1781	1781	1781
1780	1, 0	II($w = 0$)	1781	1781	1781	1781
1855	2, 2	I	1826	1816	1826	1826
2275	1, 3	I	2233	2218	2233	2233
2275	3, 1	I	2233	2218	2233	2233
2517	1, 1	II($w = 0$)	2518	2518	2518	2518
2874	3, 2	I	2815	2791	2815	2815
$a/h = 20$						
251.7	1, 1	I	251.4	251.2	251.4	251.4
623.9	1, 2	I	621.7	620.9	621.6	621.6
623.9	2, 1	I	621.7	620.9	621.6	621.6
989.3	2, 2	I	984.2	982.5	984.2	984.2
1231	1, 3	I	1222	1219	1222	1222
1231	3, 1	I	1222	1219	1222	1222
1586	3, 2	I	1573	1568	1573	1573
1586	2, 3	I	1573	1568	1573	1573
1781	1, 0	II($w = 0$)	1781	1781	1781	1781
1781	0, 1	II($w = 0$)	1781	1781	1781	1781
$a/h = 100$						
50.63	1, 1	I	50.63	50.63	50.63	50.63
126.6	2, 1	I	126.5	126.5	126.5	126.5
126.6	1, 2	I	126.5	126.5	126.5	126.5
202.4	2, 2	I	202.3	202.3	202.3	202.3
253.2	1, 3	I	252.9	252.8	252.8	252.8
253.2	3, 1	I	252.9	252.8	252.8	252.8
328.8	2, 3	I	328.6	328.5	328.6	328.6
328.8	3, 2	I	328.6	328.5	328.6	328.6
430.6	1, 4	I	429.4	429.3	429.4	429.4
430.6	4, 1	I	429.4	429.3	429.4	429.4
$a/h = 1000$						
5.064	1, 1	I	5.065	5.064	5.064	5.064
12.67	1, 2	I	12.66	12.66	12.66	12.66
12.67	2, 1	I	12.66	12.66	12.66	12.66
20.26	2, 2	I	20.26	20.26	20.26	20.26
25.35	3, 1	I	25.32	25.32	25.32	25.32
25.35	1, 3	I	25.32	25.32	25.32	25.32
32.93	3, 2	I	32.92	32.92	32.92	32.92
32.93	2, 3	I	32.92	32.92	32.92	32.92
43.15	4, 1	I	43.05	43.05	43.05	43.05
43.15	1, 4	I	43.05	43.05	43.05	43.05

Table 9 Second benchmark, simply supported sandwich plate with FGM core (p = 1.0) and several thickness ratios a/h. First ten frequencies in Hz for the present 3D exact solution and several numerical solutions

FGM core with p = 1.0						
2D FE	m, n	Mode	3D exact	GDQ-RM	GDQ-ZZ	GDQ-LW
$a/h = 10$						
494.5	1, 1	I	492.0	491.6	492.0	492.0
1193	1, 2	I	1180	1178	1180	1180
1193	2, 1	I	1180	1178	1180	1180
1757	1, 0	II($w = 0$)	1757	1757	1757	1757
1757	0, 1	II($w = 0$)	1757	1757	1757	1757
1847	2, 2	I	1819	1813	1819	1819
2262	1, 3	I	2222	2213	2222	2222
2262	3, 1	I	2222	2213	2222	2222
2483	1, 1	II($w = 0$)	2485	2485	2485	2485
2853	3, 2	I	2797	2784	2797	2797
$a/h = 20$						
252.0	1, 1	I	251.6	251.6	251.6	251.6
624.2	1, 2	I	621.9	621.5	621.9	621.9
624.2	2, 1	I	621.9	621.5	621.9	621.9
989.2	2, 2	I	984.0	983.1	984.0	984.0
1230	1, 3	I	1221	1220	1221	1221
1230	3, 1	I	1221	1220	1221	1221
1584	3, 2	I	1571	1568	1571	1571
1584	2, 3	I	1571	1568	1571	1571
1757	1, 0	II($w = 0$)	1757	1757	1757	1757
1757	0, 1	II($w = 0$)	1757	1757	1757	1757
$a/h = 100$						
50.71	1, 1	I	50.71	50.71	50.71	50.71
126.8	1, 2	I	126.7	126.7	126.7	126.7
126.8	2, 1	I	126.7	126.7	126.7	126.7
202.7	2, 2	I	202.6	202.6	202.6	202.6
253.6	3, 1	I	253.2	253.2	253.2	253.2
253.6	1, 3	I	253.2	253.2	253.2	253.2
329.3	3, 2	I	329.0	329.0	329.0	329.0
329.3	2, 3	I	329.0	329.0	329.0	329.0
431.2	1, 4	I	430.0	430.0	430.0	430.0
431.2	4, 1	I	430.0	430.0	430.0	430.0
$a/h = 1000$						
5.073	1, 1	I	5.072	5.072	5.072	5.073
12.69	2, 1	I	12.68	12.68	12.68	12.68
12.69	1, 2	I	12.68	12.68	12.68	12.68
20.29	2, 2	I	20.29	20.29	20.29	20.29
25.39	3, 1	I	25.36	25.36	25.36	25.36
25.39	1, 3	I	25.36	25.36	25.36	25.36
32.99	2, 3	I	32.97	32.97	32.97	32.97
32.99	3, 1	I	32.97	32.97	32.97	32.97
43.22	1, 4	I	43.11	43.11	43.11	43.11
43.22	4, 1	I	43.11	43.11	43.11	43.11

Table 10 Second benchmark, simply supported sandwich plate with FGM core (p = 2.0) and several thickness ratios a/h. First ten frequencies in Hz for the present 3D exact solution and several numerical solutions

FGM core with $p = 2.0$						
2D FE	m, n	Mode	3D exact	GDQ-RM	GDQ-ZZ	GDQ-LW
$a/h = 10$						
500.2	1, 1	I	497.6	498.1	497.6	497.6
1202	2, 1	I	1188	1190	1188	1188
1202	1, 2	I	1188	1190	1188	1188
1728	0, 1	II($w = 0$)	1729	1729	1729	1729
1728	1, 0	II($w = 0$)	1729	1729	1729	1729
1852	2, 2	I	1825	1829	1825	1825
2263	1, 3	I	2225	2231	2225	2225
2263	3, 1	I	2225	2231	2225	2225
2443	1, 1	II($w = 0$)	2446	2446	2446	2446
2846	3, 2	I	2793	2802	2793	2793
$a/h = 20$						
255.6	1, 1	I	255.2	255.2	255.2	255.2
632.2	1, 2	I	629.8	630.2	629.8	629.8
632.2	2, 1	I	629.8	630.2	629.8	629.8
1001	2, 2	I	995.3	996.1	995.3	995.3
1243	1, 3	I	1234	1235	1234	1234
1243	3, 1	I	1234	1235	1234	1234
1599	3, 2	I	1586	1588	1586	1586
1599	2, 3	I	1586	1588	1586	1586
1729	1, 0	II($w = 0$)	1729	1729	1729	1729
1729	0, 1	II($w = 0$)	1729	1729	1729	1729
$a/h = 100$						
51.48	1, 1	I	51.47	51.47	51.47	51.47
128.7	1, 2	I	128.6	128.6	128.6	128.6
128.7	2, 1	I	128.6	128.6	128.6	128.6
205.8	2, 2	I	205.7	205.7	205.7	205.7
257.4	1, 3	I	257.0	257.0	257.0	257.0
257.4	3, 1	I	257.0	257.0	257.0	257.0
334.2	2, 3	I	333.9	333.9	333.9	333.9
334.2	3, 2	I	333.9	333.9	333.9	333.9
437.6	1, 4	I	436.3	436.4	436.3	436.3
437.6	4, 1	I	436.3	436.4	436.3	436.3
$a/h = 1000$						
5.149	1, 1	I	5.149	5.149	5.149	5.149
12.88	1, 2	I	12.87	12.87	12.87	12.87
12.88	2, 1	I	12.87	12.87	12.87	12.87
20.60	2, 2	I	20.60	20.60	20.60	20.60
25.78	3, 1	I	25.74	25.74	25.74	25.74
25.78	1, 3	I	25.74	25.74	25.74	25.74
33.49	3, 2	I	33.47	33.47	33.47	33.47
33.49	2, 3	I	33.47	33.47	33.47	33.47
43.87	4, 1	I	43.76	43.77	43.77	43.77
43.87	1, 4	I	43.76	43.77	43.77	43.77

Table 11 Third benchmark, simply supported one-layered FGM cylinder with $p = 0.0$ and several thickness ratios R_x/h. First ten frequencies in Hz for the present 3D exact solution and several numerical solutions

$p = 0.0$						
2D FE	m, n	Mode	3D exact	GDQ-RM	GDQ-ESL	GDQ-LW
$R_x/h = 5$						
70.25	4, 1	I	70.21	70.51	70.20	70.20
93.34	6, 1	I	93.34	93.44	93.34	93.34
97.76	2, 1	I	97.76	97.79	97.76	97.76
98.77	2, 0	I($w = 0$)	98.87	98.82	98.69	98.85
147.4	8, 1	I	146.7	146.3	146.7	146.7
155.7	0, 1	I($w = 0$)	155.0	155.0	155.0	155.0
155.9	4, 2	I	153.7	153.9	153.7	153.7
156.5	0, 1	II($w = 0$)	156.0	155.8	156.0	156.0
168.9	6, 2	I	167.2	167.1	167.2	167.2
169.0	2, 2	I	166.0	166.1	166.0	166.0
$R_x/h = 10$						
56.39	6, 1	I	56.25	56.40	56.25	56.25
59.22	4, 1	I	59.12	59.24	59.12	59.12
81.46	8, 1	I	81.11	81.16	81.11	81.11
96.16	2, 1	I	96.13	96.14	96.13	96.13
98.74	2, 0	I($w = 0$)	98.74	98.76	98.74	98.72
113.9	6, 2	I	113.0	113.2	113.0	113.0
120.8	10, 1	I	119.9	119.7	119.9	119.9
124.1	4, 2	I	123.2	123.3	123.2	123.2
126.4	8, 2	I	125.5	125.6	125.5	125.5
149.3	2, 2	I	148.3	148.4	148.3	148.3
$R_x/h = 100$						
18.82	10, 1	I	18.72	18.73	18.72	18.72
20.54	12, 1	I	20.39	20.40	20.39	20.39
22.17	8, 1	I	22.09	22.10	22.09	22.09
25.40	14, 1	I	25.16	25.17	25.16	25.16
32.17	16, 1	I	31.76	31.77	31.77	31.77
32.74	6, 1	I	32.66	32.66	32.66	32.66
38.48	14, 2	I	38.09	38.10	38.09	38.09
40.21	18, 1	I	39.67	39.67	39.67	39.67
40.32	12, 2	I	39.84	39.85	39.84	39.84
41.08	16, 2	I	40.60	40.61	40.60	40.60
$R_x/h = 1000$						
6.223	18, 1	I	6.116	6.117	6.117	6.117
6.308	20, 1	I	6.178	6.178	6.178	6.178
6.734	16, 1	I	6.641	6.642	6.642	6.642
6.842	22, 1	I	6.671	6.672	6.672	6.672
7.701	24, 1	I	7.473	7.474	7.474	7.474
8.008	14, 1	I	7.922	7.922	7.922	7.922
8.802	26, 1	I	8.497	8.495	8.495	8.495
10.09	28, 1	I	9.688	9.701	9.700	9.700
10.30	12, 1	I	10.21	10.21	10.21	10.21
11.55	30, 1	I	11.02	11.10	11.10	11.10

Table 12 Third benchmark, simply supported one-layered FGM cylinder with $p = 0.5$ and thickness ratios R_α/h. First ten frequencies in Hz for the present 3D exact solution and several numerical solutions

$p = 0.5$						
2D FE	m, n	Mode	3D exact	GDQ-RM	GDQ-ESL	GDQ-LW
$R_\alpha/h = 5$						
61.50	4, 1	I	61.53	61.75	61.53	61.53
78.76	6, 1	I	78.94	78.84	78.92	78.93
87.72	2, 0	I($w = 0$)	87.65	87.62	87.47	87.62
87.81	2, 1	I	87.47	87.60	87.15	87.47
123.5	8, 1	I	123.3	122.5	123.3	123.3
135.7	4, 2	I	133.6	133.7	133.5	133.5
139.0	0, 1	I	137.4	137.6	137.4	137.4
142.2	0, 1	II($w = 0$)	140.9	140.9	140.9	140.9
144.8	6, 2	I	143.3	143.1	143.3	143.3
148.5	2, 2	I	145.1	145.4	145.1	145.1
$R_\alpha/h = 10$						
48.37	6, 1	I	48.35	48.43	48.34	48.34
52.61	4, 1	I	52.56	52.66	52.56	52.56
68.56	8, 1	I	68.44	68.37	68.43	68.43
86.26	2, 1	I	86.07	86.13	86.07	86.07
88.03	2, 0	I($w = 0$)	87.96	87.99	87.96	87.95
98.95	6, 2	I	98.23	98.37	98.22	98.22
101.4	10, 1	I	100.9	100.6	100.8	100.8
107.9	8, 2	I	107.3	107.2	107.2	107.2
109.6	4, 2	I	108.7	108.8	108.6	108.6
132.6	2, 2	I	131.3	131.5	131.3	131.3
$R_\alpha/h = 100$						
16.42	10, 1	I	16.35	16.35	16.35	16.35
17.60	12, 1	I	17.49	17.49	17.48	17.48
19.70	8, 1	I	19.63	19.64	19.63	19.63
21.56	14, 1	I	21.37	21.37	21.37	21.37
27.21	16, 1	I	26.89	26.89	26.89	26.89
29.26	6, 1	I	29.20	29.21	29.20	29.20
33.44	14, 2	I	33.11	33.12	33.11	33.11
34.06	18, 1	I	33.54	33.53	33.54	33.54
35.26	16, 2	I	34.86	34.87	34.86	34.86
35.42	12, 2	I	35.11	35.12	35.11	35.11
$R_\alpha/h = 1000$						
5.442	20, 1	I	5.342	5.342	5.342	5.342
5.453	18, 1	I	5.351	5.351	5.351	5.351
5.861	22, 1	I	5.719	5.717	5.717	5.717
5.954	16, 1	I	5.874	5.873	5.873	5.873
6.559	24, 1	I	6.369	6.368	6.368	6.368
7.131	14, 1	I	7.056	7.055	7.055	7.055
7.471	26, 1	I	7.217	7.213	7.213	7.213
8.551	28, 1	I	8.213	8.222	8.222	8.222
9.201	12, 1	I	9.128	9.127	9.127	9.127
9.775	30, 1	I	9.330	9.395	9.396	9.396

Table 13 Third benchmark, simply supported one-layered FGM cylinder with $p = 1.0$ and several thickness ratios R_α/h. First ten frequencies in Hz for the present 3D exact solution and several numerical solutions

$p = 1.0$						
2D FE	m, n	Mode	3D exact	GDQ-RM	GDQ-ESL	GDQ-LW
$R_\alpha/h = 5$						
56.37	4, 1	I	56.43	56.63	56.43	56.43
70.80	6, 1	I	71.05	70.95	71.05	71.05
80.88	2, 0	I($w = 0$)	80.77	80.76	80.75	80.70
81.44	2, 1	I	80.97	81.15	80.97	80.97
110.5	8, 1	I	110.5	109.8	110.5	110.5
123.9	4, 2	I	121.8	122.0	121.8	121.8
128.2	0, 1	I	126.1	126.5	126.1	126.1
131.0	6, 2	I	129.8	129.6	129.8	129.8
133.1	0, 1	II($w = 0$)	131.7	131.7	131.7	131.7
136.2	2, 2	I	132.8	133.1	132.8	132.8
$R_\alpha/h = 10$						
43.91	6, 1	I	43.93	43.99	43.93	43.93
48.56	4, 1	I	48.53	48.62	48.53	48.53
61.64	8, 1	I	61.58	61.49	61.58	61.58
79.96	2, 1	I	79.70	79.79	79.70	79.70
81.33	2, 0	I($w = 0$)	81.24	81.23	81.17	81.24
90.36	6, 2	I	89.70	89.83	89.70	89.70
90.95	10, 1	I	90.56	90.27	90.56	90.56
97.64	8, 2	I	97.11	97.10	97.11	97.11
100.9	4, 2	I	99.88	100.1	99.88	99.88
120.3	10, 2	I	119.6	119.3	119.6	119.6
$R_\alpha/h = 100$						
15.04	10, 1	I	14.97	14.97	14.97	14.97
15.98	12, 1	I	15.87	15.87	15.87	15.87
18.18	8, 1	I	18.12	18.12	18.12	18.12
19.49	14, 1	I	19.31	19.31	19.31	19.31
24.55	16, 1	I	24.26	24.25	24.26	24.26
27.08	6, 1	I	27.03	27.03	27.03	27.03
30.56	18, 1	I	30.24	30.23	30.24	30.24
30.72	14, 2	I	30.26	30.26	30.26	30.26
32.04	16, 2	I	31.67	31.68	31.67	31.67
32.57	12, 2	I	32.28	32.29	32.28	32.28
$R_\alpha/h = 1000$						
4.972	20, 1	I	4.869	4.869	4.869	4.869
4.989	18, 1	I	4.905	4.904	4.904	4.904
5.321	22, 1	I	5.189	5.189	5.189	5.189
5.484	16, 1	I	5.408	5.409	5.408	5.408
5.938	24, 1	I	5.764	5.763	5.763	5.763
6.588	26, 1	I	6.520	6.518	6.518	6.518
6.753	14, 1	I	6.517	6.517	6.517	6.517
7.723	28, 1	I	7.413	7.422	7.422	7.422
8.512	30, 1	I	8.417	8.443	8.443	8.443
8.823	12, 1	I	8.443	8.477	8.477	8.477

Table 14 Third benchmark, simply supported one-layered FGM cylinder with $p = 2.0$ and several thickness ratios R_α/h. First ten frequencies in Hz for the present 3D exact solution and several numerical solutions

$p = 2.0$						
2D FE	m, n	Mode	3D exact	GDQ-RM	GDQ-ESL	GDQ-LW
$R_\alpha/h = 5$						
50.94	4, 1	I	51.05	51.26	51.05	51.05
63.65	6, 1	I	64.07	64.08	64.07	64.07
72.77	2, 0	I($w = 0$)	72.67	72.67	72.69	72.67
73.72	2, 1	I	73.20	73.42	73.20	73.20
98.89	8, 1	I	99.24	98.99	99.24	99.24
111.7	4, 2	I	109.8	110.1	109.8	109.8
115.4	0, 1	I	113.1	113.5	113.1	113.1
117.8	6, 2	I	116.9	117.1	116.9	116.9
121.2	0, 1	II($w = 0$)	119.9	119.9	119.4	119.4
122.8	2, 2	I	119.4	128.4	127.9	127.9
$R_\alpha/h = 10$						
39.71	6, 1	I	39.78	39.84	39.78	39.78
43.90	4, 1	I	43.88	43.98	43.88	43.88
55.69	8, 1	I	55.75	55.70	55.75	55.74
72.30	2, 1	I	72.02	72.12	72.02	71.90
73.32	2, 0	I($w = 0$)	73.23	73.20	73.19	72.34
81.68	6, 2	I	81.10	81.26	81.10	81.09
82.06	10, 1	I	81.89	81.73	81.89	81.89
88.23	8, 2	I	87.83	87.92	87.84	87.83
91.11	4, 2	I	90.16	90.38	90.17	90.15
108.6	10, 2	I	108.1	108.0	108.1	108.1
$R_\alpha/h = 100$						
13.63	10, 1	I	13.56	13.57	13.56	13.56
14.51	12, 1	I	14.41	14.42	14.41	14.41
16.43	8, 1	I	16.38	16.38	16.38	16.38
17.72	14, 1	I	17.56	17.56	17.56	17.56
22.33	16, 1	I	22.07	22.07	22.07	22.07
24.46	6, 1	I	24.41	24.41	24.41	24.41
27.70	14, 2	I	27.42	27.43	27.43	27.43
27.94	18, 1	I	27.51	27.51	27.51	27.51
29.08	16, 2	I	28.75	28.76	28.75	28.75
29.47	12, 2	I	29.21	29.21	29.21	29.21
$R_\alpha/h = 1000$						
4.511	20, 1	I	4.418	4.418	4.418	4.418
4.519	18, 1	I	4.443	4.442	4.442	4.442
4.835	22, 1	I	4.715	4.714	4.714	4.714
4.960	16, 1	I	4.891	4.892	4.891	4.891
5.400	24, 1	I	5.241	5.241	5.241	5.241
5.953	26, 1	I	5.888	5.888	5.888	5.888
6.144	14, 1	I	5.932	5.930	5.930	5.930
7.028	28, 1	I	6.747	6.755	6.755	6.755
7.688	12, 1	I	7.625	7.626	7.625	7.625
8.031	30, 1	I	7.662	7.717	7.717	7.717

Table 15 Fourth benchmark, simply supported cylinder with classical core and several thickness ratios R_α/h. First ten frequencies in Hz for the present 3D exact solution and several numerical solutions

Classical core						
2D FE	m, n	Mode	3D exact	GDQ-RM	GDQ-ZZ	GDQ-LW
$R_\alpha/h = 5$						
39.43	4, 1	I	39.42	39.58	39.42	39.38
51.34	6, 1	I	51.41	51.45	51.42	51.47
55.62	2, 1	I	55.35	55.38	55.35	55.27
55.64	2, 0	I($w = 0$)	55.45	55.48	55.45	55.48
80.64	8, 1	I	80.45	80.22	80.48	80.61
87.23	4, 2	I	85.90	86.04	85.91	85.87
88.22	0, 1	I	87.37	87.36	87.38	87.39
89.72	0, 1	II	88.27	88.27	88.27	88.14
93.72	6, 2	I	92.81	92.84	92.84	92.84
94.93	2, 2	I	92.90	93.01	92.91	92.85
$R_\alpha/h = 10$						
31.35	6, 1	I	31.32	34.09	31.32	31.31
33.47	4, 1	I	33.43	35.24	33.43	33.40
44.87	8, 1	I	44.76	49.34	44.76	44.76
54.62	2, 1	I	54.46	55.66	54.46	54.42
55.79	2, 0	I($w = 0$)	55.67	56.36	55.63	55.66
63.71	6, 2	I	63.24	68.06	63.25	63.21
66.43	10, 1	I	66.03	72.88	66.04	66.04
69.93	4, 2	I	69.34	73.37	69.35	69.31
70.12	8, 2	I	69.69	76.16	69.69	69.67
84.30	2, 2	I	83.53	87.59	83.53	83.49
$R_\alpha/h = 100$						
10.59	10, 1	I	10.51	10.51	10.51	10.51
11.44	12, 1	I	11.36	11.37	11.37	11.36
12.53	8, 1	I	12.49	12.49	12.49	12.49
14.10	14, 1	I	13.97	13.98	13.97	13.97
17.84	16, 1	I	17.62	17.62	17.62	17.62
18.54	6, 1	I	18.51	18.51	18.51	18.50
21.56	14, 2	I	21.34	21.35	21.34	21.34
22.34	18, 1	I	21.99	21.99	21.99	21.99
22.64	12, 2	I	22.44	22.45	22.44	22.44
22.90	16, 2	I	22.64	22.65	22.64	22.64
$R_\alpha/h = 1000$						
3.496	18, 1	I	3.436	3.685	3.436	3.436
3.528	20, 1	I	3.455	3.746	3.455	3.455
3.799	22, 1	I	3.719	3.975	3.719	3.719
3.813	16, 1	I	3.746	4.066	3.746	3.746
4.283	24, 1	I	4.157	4.569	4.157	4.157
4.530	14, 1	I	4.480	4.721	4.481	4.481
4.889	26, 1	I	4.720	5.202	4.718	4.718
5.603	28, 1	I	5.377	5.946	5.385	5.385
5.832	12, 1	I	5.785	6.074	5.785	5.785
6.408	30, 1	I	6.113	6.805	6.157	6.157

Table 16 Fourth benchmark, simply supported sandwich cylinder with FGM core ($p = 0.5$) and several thickness ratios R_α/h. First ten frequencies in Hz for the present 3D exact solution and several numerical solutions

FGM core with $p = 0.5$						
2D FE	m, n	Mode	3D exact	GDQ-RM	GDQ-ZZ	GDQ-LW
$R_\alpha/h = 5$						
39.22	4, 1	I	39.24	39.35	39.24	39.23
49.79	6, 1	I	49.98	49.88	49.97	50.11
56.25	2, 0	I($w = 0$)	55.97	55.99	55.95	55.89
56.34	2, 1	I	55.95	56.02	55.96	55.96
78.01	8, 1	I	78.03	77.52	78.04	78.30
86.42	4, 2	I	85.09	85.09	85.09	85.13
89.13	0, 1	I	88.12	88.12	88.12	88.14
91.44	0, 1	II	89.54	90.79	91.02	91.15
91.84	6, 2	I	91.02	92.78	92.73	92.76
94.84	2, 2	I	92.73	99.71	99.68	99.73
$R_\alpha/h = 10$						
30.68	6, 1	I	30.69	30.74	30.69	30.70
33.68	4, 1	I	33.65	33.71	33.65	33.63
43.27	8, 1	I	43.24	43.19	43.24	43.29
55.36	2, 1	I	55.15	55.17	55.15	55.12
56.47	2, 0	I($w = 0$)	56.30	56.22	56.39	56.28
62.98	6, 2	I	62.56	62.62	62.56	62.56
63.93	10, 1	I	63.70	63.50	63.70	63.77
68.33	8, 2	I	67.99	67.96	67.99	68.03
70.08	4, 2	I	69.49	69.56	69.48	69.47
84.41	10, 2	I	83.96	83.76	83.96	84.03
$R_\alpha/h = 100$						
10.46	10, 1	I	10.41	10.42	10.41	10.41
11.14	12, 1	I	11.07	11.07	11.07	11.07
12.61	8, 1	I	12.57	12.57	12.57	12.57
13.61	14, 1	I	13.49	13.49	13.49	13.49
17.16	16, 1	I	16.96	16.95	16.95	16.96
18.77	6, 1	I	18.74	18.74	18.74	18.73
21.27	14, 2	I	21.06	21.07	21.06	21.06
22.47	18, 1	I	21.14	21.14	21.14	21.14
22.34	16, 2	I	22.09	22.09	22.09	22.09
22.62	12, 2	I	22.42	22.43	22.42	22.42
$R_\alpha/h = 1000$						
3.462	20, 1	I	3.391	3.391	3.391	3.391
3.468	18, 1	I	3.410	3.410	3.409	3.409
3.710	22, 1	I	3.618	3.618	3.618	3.618
3.807	16, 1	I	3.755	3.755	3.755	3.755
4.144	24, 1	I	4.022	4.022	4.022	4.022
4.569	14, 1	I	4.520	4.520	4.520	4.520
4.715	26, 1	I	4.553	4.551	4.551	4.551
5.393	28, 1	I	5.178	5.185	5.185	5.185
5.901	12, 1	I	5.854	5.854	5.854	5.854
6.163	30, 1	I	5.880	5.922	5.922	5.922

Table 17 Fourth benchmark, simply supported sandwich cylinder with FGM core (p = 1.0) and several thickness ratios R_α/h. First ten frequencies in Hz for the present 3D exact solution and several numerical solutions

FGM core with p = 1.0						
2D FE	m, n	Mode	3D exact	GDQ-RM	GDQ-ZZ	GDQ-LW
$R_\alpha/h = 5$						
38.87	4, 1	I	38.90	39.02	38.90	38.92
49.45	6, 1	I	49.73	49.67	49.73	49.94
55.42	2, 0	I($w = 0$)	55.09	55.06	55.09	55.10
55.70	2, 1	I	55.24	55.29	55.24	55.18
77.35	8, 1	I	77.56	77.19	77.57	77.97
85.63	4, 2	I	84.28	84.34	84.28	84.39
87.85	0, 1	I	86.71	86.73	86.71	86.72
90.66	0, 1	II	88.51	88.51	88.51	88.39
91.08	6, 2	I	90.33	90.24	90.34	90.59
93.80	2, 2	I	91.58	91.66	91.58	91.65
$R_\alpha/h = 10$						
30.50	6, 1	I	30.54	30.59	30.54	30.58
33.31	4, 1	I	33.28	33.34	33.28	33.27
43.12	8, 1	I	43.16	43.11	43.16	43.25
54.68	2, 1	I	54.43	54.45	54.43	54.40
55.68	2, 0	I($w = 0$)	55.49	55.31	55.45	55.44
62.49	6, 2	I	62.09	62.16	62.09	62.12
63.71	10, 1	I	63.57	63.41	63.57	63.71
67.98	8, 2	I	67.70	67.69	67.70	67.78
69.33	4, 2	I	68.71	68.79	68.71	68.70
83.91	10, 2	I	83.69	83.08	83.01	82.99
$R_\alpha/h = 100$						
10.39	10, 1	I	10.34	10.34	10.34	10.34
11.11	12, 1	I	11.04	11.04	11.04	11.04
12.47	8, 1	I	12.43	12.43	12.43	12.43
13.61	14, 1	I	13.49	13.49	13.49	13.49
17.17	16, 1	I	16.97	16.97	16.97	16.97
18.53	6, 1	I	18.50	18.50	18.50	18.49
21.14	14, 2	I	20.93	20.94	20.93	20.93
21.49	18, 1	I	21.16	21.16	21.16	21.17
22.27	16, 2	I	22.02	22.02	22.02	22.02
22.41	12, 2	I	22.21	22.22	22.21	22.21
$R_\alpha/h = 1000$						
3.442	20, 1	I	3.376	3.376	3.375	3.376
3.447	18, 1	I	3.384	3.384	3.384	3.384
3.703	22, 1	I	3.611	3.611	3.611	3.611
3.768	16, 1	I	3.716	3.717	3.717	3.716
4.142	24, 1	I	4.020	4.020	4.020	4.020
4.515	14, 1	I	4.466	4.466	4.466	4.466
4.717	26, 1	I	4.554	4.553	4.553	4.553
5.399	28, 1	I	5.182	5.189	5.189	5.189
5.826	12, 1	I	5.779	5.779	5.779	5.779
6.171	30, 1	I	5.887	5.929	5.929	5.929

Table 18 Fourth benchmark, simply supported sandwich cylinder with FGM core (p = 2.0) and several thickness ratios R_α/h. First ten frequencies in Hz for the present 3D exact solution and several numerical solutions

FGM core with p = 2.0						
2D FE	m, n	Mode	3D exact	GDQ-RM	GDQ-ZZ	GDQ-LW
$R_\alpha/h = 5$						
38.61	4, 1	I	38.67	38.81	38.67	38.70
49.53	6, 1	I	49.90	49.97	49.91	50.19
54.47	2, 0	I($w = 0$)	54.13	54.09	54.13	54.14
54.92	2, 1	I	54.44	54.49	54.44	54.37
77.37	8, 1	I	77.75	77.74	77.75	78.28
85.11	4, 2	I	83.76	83.97	83.76	83.93
86.41	0, 1	I	85.17	85.21	85.17	85.18
89.52	0, 1	II	87.25	90.38	87.23	87.10
90.83	6, 2	I	90.16	90.39	90.16	90.52
92.87	2, 2	I	90.57	90.72	90.57	90.67
$R_\alpha/h = 10$						
30.55	6, 1	I	30.62	30.67	30.62	30.67
32.92	4, 1	I	32.90	32.95	32.90	32.88
43.47	8, 1	I	43.56	43.56	43.56	43.68
53.85	2, 1	I	53.59	53.61	53.59	53.55
54.77	2, 0	I($w = 0$)	54.56	54.45	54.55	54.55
62.27	6, 2	I	61.88	61.99	61.88	61.94
64.21	10, 1	I	64.16	64.11	64.16	64.36
68.18	8, 2	I	67.94	68.03	67.94	67.99
68.62	4, 2	I	67.99	68.08	67.99	68.08
82.79	10, 2	I	81.84	81.91	81.84	81.81
$R_\alpha/h = 100$						
10.35	10, 1	I	10.31	10.31	10.31	10.31
11.19	12, 1	I	11.12	11.12	11.12	11.12
12.32	8, 1	I	12.28	12.28	12.28	12.28
13.77	14, 1	I	13.65	13.65	13.65	13.65
17.41	16, 1	I	17.20	17.20	17.20	17.21
18.25	6, 1	I	18.21	18.22	18.21	18.21
21.12	14, 2	I	20.92	20.92	20.92	20.92
21.80	18, 1	I	21.47	21.46	21.47	21.47
22.23	12, 2	I	22.04	22.05	22.04	22.04
22.40	16, 2	I	22.15	22.16	22.15	22.16
$R_\alpha/h = 1000$						
3.429	18, 1	I	3.371	3.371	3.371	3.371
3.455	20, 1	I	3.384	3.384	3.384	3.384
3.730	22, 1	I	3.638	3.638	3.638	3.638
3.732	16, 1	I	3.681	3.681	3.681	3.681
4.187	24, 1	I	4.063	4.063	4.063	4.064
4.455	14, 1	I	4.407	4.407	4.407	4.407
4.777	26, 1	I	4.611	4.610	4.610	4.611
5.472	28, 1	I	5.253	5.260	5.260	5.260
5.739	12, 1	I	5.692	5.693	5.693	5.693
6.258	30, 1	I	5.970	6.013	6.014	6.014

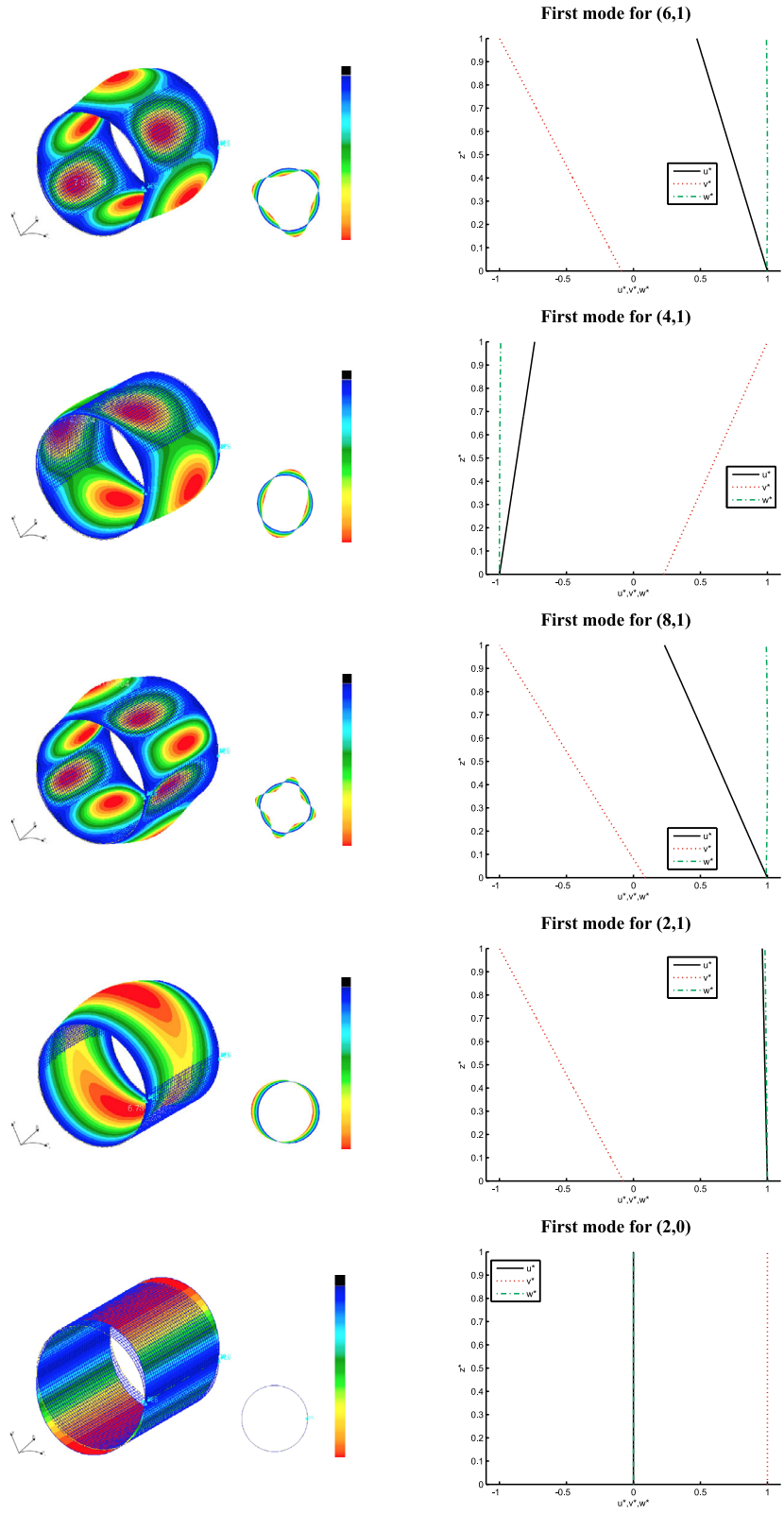

Fig. 11 Fourth benchmark, simply supported sandwich cylinder with FGM core ($p = 0.5$) and thickness ratio $R_\alpha/h = 10$. First five frequencies via 2D FE solution (on the *left*) and via 3D exact solution (on the *right*)

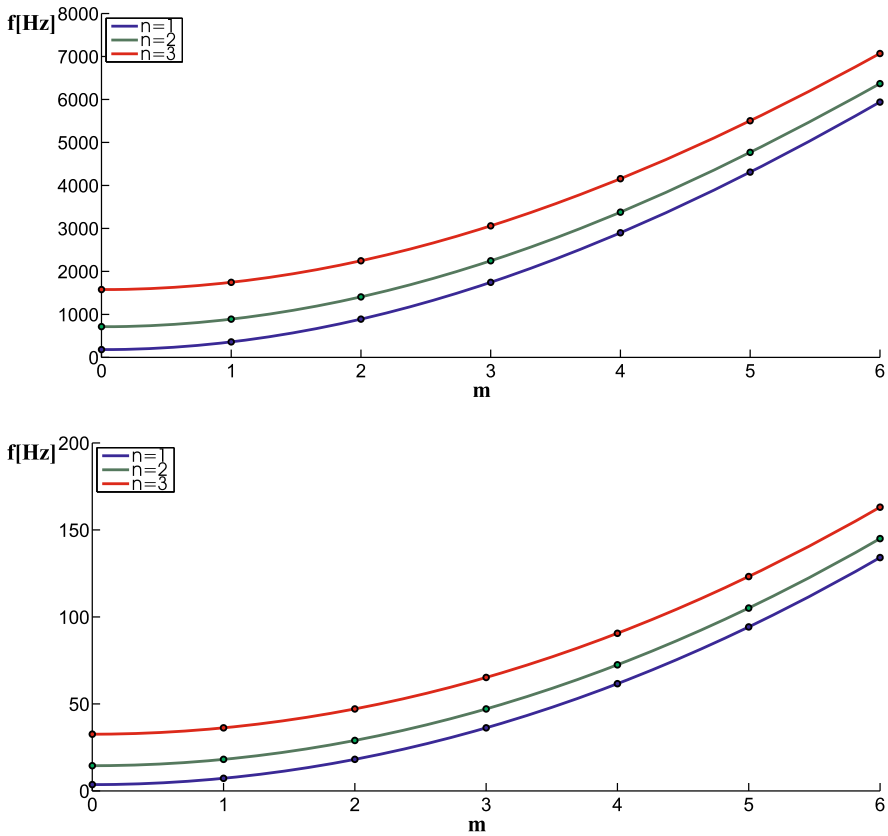

Fig. 12 First benchmark, simply supported FGM plate with $p = 1.0$ and thickness ratios $a/h = 10$ (at the *top*) and $a/h = 1000$ (at the *bottom*). First (I) 3D frequencies versus half-wave numbers m (from 0 to 6) and n (from 1 to 3)

numbers m and n. A sufficiently high number of nodes must be considered in order to describe high order mode shapes. In the case of one-layered structures (see also the one-layered FGM plate in Tables 3, 4, 5, 6), there are no differences between the ESL model and the LW model. 2D FE model and GDQ-RM model have some difficulties for thick cylinders and/or higher frequencies because they use a simplified kinematic model such as the Reissner–Mindlin model. GDQ-ESL and GDQ-LW models are always very similar to 3D exact results because of the refined kinematic model used to approximate the displacement components through the thickness direction. Some in-plane vibration modes with zero transverse displacement w are present in the first ten frequencies of Tables 11, 12, 13 and 14 when thick cylinders are considered (thickness ratios R_α/h equals 5 or 10). In Tables 11 and 12, in the case of thick cylinders ($R_\alpha/h = 5$), the difficulties of the 2D FE model is confirmed by the fact that some frequencies are exchanged (e.g., the sixth and seventh frequencies in Table 11 and the ninth and tenth frequency in Table 11 for $p = 0$ and $R_\alpha/h = 5$, or the third and fourth frequencies in Table 12 for $p = 0.5$ and $R_\alpha/h = 5$).

Tables 15, 16, 17 and 18 show the first ten frequencies for the sandwich cylinder with FGM core. The FGM sandwich configuration is the same already seen for the plate case. All the considerations already seen for the other plate and cylinder cases (Tables 3, 4, 5, 6, 7, 8, 9, 10, 11, 12, 13, 14) are here still valid. 2D FE and GDQ-RM models have some difficulties for thick cylinders and/or higher frequencies. The use of 2D refined models (GDQ-ZZ and GDQ-LW) is mandatory to obtain the 3D exact frequencies for each thickness ratio R_α/h, for each FGM law of the core and for both lower and higher frequency orders. In the case of cylinder geometry and multilayer configuration, LW models have some difficulties with respect to the ESL models (with and without the zigzag Murakami function) to impose the correct simply supported boundary conditions. For this reason in Tables 15, 16, 17 and 18 there are some differences between the GDQ-ZZ model and the GDQ-LW model. Figure 11 shows an example for the first five vibration modes

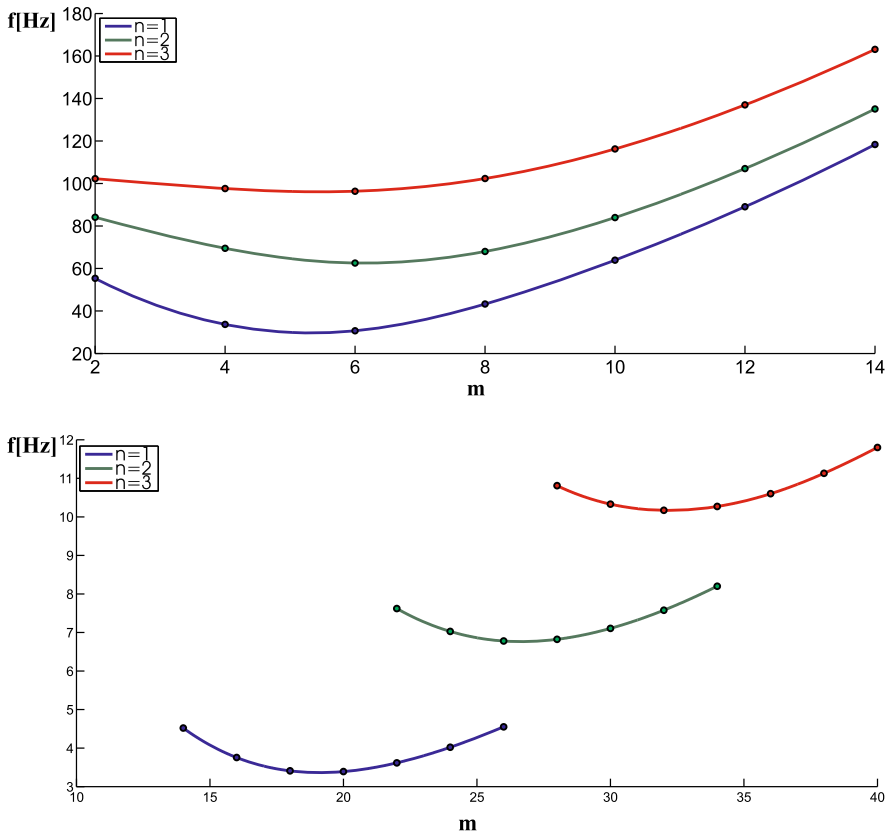

Fig. 13 Fourth benchmark, simply supported sandwich cylinder with FGM core (p = 0.5) and thickness ratios $R_\alpha/h = 10$ (at the *top*) and $R_\alpha/h = 1000$ (at the *bottom*). First (I) 3D frequencies versus half-wave numbers m (values around that for minimum frequency) and n (from 1 to 3)

obtained via the 2D FE model. A thick cylinder ($R_\alpha/h = 10$) and an FGM law with p = 0.5 are considered. The 2D FE modes are in the left column and the exact 3D vibration modes are in the right column. From both 2D FE and 3D exact vibration modes is clear how the fifth frequency is an in-plane vibration mode with zero transverse displacement w.

Figures 12 and 13 show a 3D exact analysis for a simply supported FGM plate with p = 1.0 and a simply supported sandwich FGM cylinder with p = 0.5, respectively. In Fig. 12, the 3D exact model is used to investigate the first natural frequency (I) when the half-wave number n varies from 1 to 3 and the half-wave number m varies from 0 to 6. The frequency value increases when the m value increases. Each curve f versus m move to higher frequency values when the n half-wave number increases. The cylinder case is analyzed in Fig. 13, the 3D exact model is used to investigate the first natural frequency (I) when the longitudinal half-wave number n varies from 1 to 3 and the circumferential half-wave number m varies around the minimum value. The coupling due to the curvature effect gives curves which have a minimum of frequency for a m value different from 0 or 1. Such curves f versus m move to higher frequency value when the longitudinal half-wave number n increases. These curves have a minimum in frequency moved to higher m values. Figures 12 and 13 are useful to understand the differences between the plate and cylinder behavior, these differences are due to the curvature coupling.

6 Conclusions

An exact three-dimensional model and several refined and classical two-dimensional generalized differential quadrature (GDQ) methods have been proposed for the free vibration analysis of one-layered and sandwich plates and cylinders embedding functionally graded material (FGM) layers. Finite element (FE) results have also been proposed in order to explain the

method used for the comparison between exact 3D and numerical 2D models and also to see the possible differences between an exact 3D solution and numerical 2D solutions.

The exact 3D solution gives infinite vibration modes from I to ∞ (for all the possible combinations of half-wave numbers (m, n)). A 2D numerical code gives a finite number of vibration modes because it uses a finite number of degrees of freedom in the plane and in the thickness direction. A possible method to make a 3D versus 2D comparison is to calculate the frequencies via the 2D numerical code (e.g., the 2D FE code) and then to evaluate the 3D exact frequencies by means of the appropriate half-wave numbers (obtained via a correct visualization of the vibration modes via the FE method). The 3D analysis could give some frequencies that are missed by the 2D numerical codes, but this investigation is not the main aim of the present paper. The paper tries to explain what could be the advantages and the limitations of 2D numerical codes. A typical 2D FE code uses a Reissner–Mindlin model for the approximation of displacement components through the thickness direction. Results in this paper show how this model employed by commercial FE codes could give errors for thick and moderately thick structures, complicated FGM laws and multilayered configurations, higher order frequencies and particular vibration modes. In all these cases, the use of refined 2D GDQ models is mandatory to obtain the 3D exact frequencies.

The behavior of frequency values and vibration modes versus imposed half-wave numbers has been investigated via the 3D exact model. The behavior is simple and easily predictable for plate structures because the increasing of m and/or n values gives larger frequency values. In the case of cylinder geometry there is a coupling between the displacement components due to the curvature R_α. For this reason, when the half-wave number n is imposed, the minimum of frequency is obtained for a value of the half-wave number m different from 0 or 1. When the half-wave number n increases, the frequency versus m curves move to higher values of frequencies and the minimum in frequency moves to higher values of the half-wave number m. These last considerations are very similar for one-layered and sandwich FGM cylinders.

References

1. Birman V, Byrd LW (2007) Modeling and analysis of functionally graded materials and structures. Appl Mech Rev 60:195–216
2. Dong L, Atluri SN (2011) A simple procedure to develop efficient & stable hybrid/mixed elements, and Voronoi cell finite elements for macro- & micro-mechanics. CMC Comput Mater Contin 24:61–104
3. Bishay PL, Sladek J, Sladek V, Atluri SN (2012) Analysis of functionally graded magneto-electro-elastic composites using hybrid/mixed finite elements and node-wise material properties. CMC Comput Mater Contin 29:213–262
4. Bishay PL, Atluri SN (2012) High-performance 3D hybrid/mixed, and simple 3D Voronoi cell finite elements, for macro- & micro-mechanical modeling of solids, without using multi-field variational principles. CMES Comput Model Eng Sci 84:41–97
5. Brischetto S (2009) Classical and mixed advanced models for sandwich plates embedding functionally graded cores. J Mech Mater Struct 4:13–33
6. Carrera E, Brischetto S (2009) A survey with numerical assessment of classical and refined theories for the analysis of sandwich plates. Appl Mech Rev 62:1–17
7. Brischetto S, Leetsch R, Carrera E, Wallmersperger T, Kröplin B (2008) Thermo-mechanical bending of functionally graded plates. J Therm Stress 31:286–308
8. Mattei G, Tirella A, Ahluwalia A (2012) Functionally Graded Materials (FGMs) with predictable and controlled gradient profiles: computational modelling and realisation. CMES Comput Model Eng Sci 87:483–504
9. Thai HT, Kim SE (2015) A review of theories for the modeling and analysis of functionally graded plates and shells. Compos Struct 128:70–86
10. Swaminathan K, Naveenkumar DT, Zenkour AM, Carrera E (2015) Stress, vibration and buckling analyses of FGM plates—a state-of-the-art review. Compos Struct 120:10–31
11. Carrera E, Brischetto S, Robaldo A (2008) Variable kinematic model for the analysis of functionally graded material plates. AIAA J 46:194–203
12. Brischetto S, Carrera E (2010) Advanced mixed theories for bending analysis of functionally graded plates. Comput Struct 88:1474–1483
13. Brischetto S (2013) Exact elasticity solution for natural frequencies of functionally graded simply-supported structures. CMES Comput Model Eng Sci 95:391–430
14. Dong CY (2008) Three-dimensional free vibration analysis of functionally graded annular plates using the Chebyshev-Ritz method. Mater Des 29:1518–1525
15. Li Q, Iu VP, Kou KP (2008) Three-dimensional vibration analysis of functionally graded material sandwich plates. J Sound Vib 311:498–515
16. Malekzadeh P (2009) Three-dimensional free vibration analysis of thick functionally graded plates on elastic foundations. Compos Struct 89:367–373
17. Hosseini-Hashemi S, Salehipour H, Atashipour SR (2012) Exact three-dimensional free vibration analysis of thick homogeneous plates coated by a functionally graded layer. Acta Mech 223:2153–2166

18. Vel SS, Batra RC (2004) Three-dimensional exact solution for the vibration of functionally graded rectangular plates. J Sound Vib 272:703–730
19. Kashtalyan M (2004) Three-dimensional elasticity solution for bending of functionally graded rectangular plates. Eur J Mech A/Solids 23:853–864
20. Xu Y, Zhou D (2009) Three-dimensional elasticity solution of functionally graded rectangular plates with variable thickness. Compos Struct 91:56–65
21. Kashtalyan M, Menshykova M (2009) Three-dimensional elasticity solution for sandwich panels with a functionally graded core. Compos Struct 87:36–43
22. Zhong Z, Shang ET (2003) Three-dimensional exact analysis of a simply supported functionally gradient piezoelectric plate. Int J Solids Struct 40:5335–5352
23. Alibeigloo A, Kani AM, Pashaei MH (2012) Elasticity solution for the free vibration analysis of functionally graded cylindrical shell bonded to thin piezoelectric layers. Int J Press Vessels Pip 89:98–111
24. Zahedinejad P, Malekzadeh P, Farid M, Karami G (2010) A semi-analytical three-dimensional free vibration analysis of functionally graded curved panels. Int J Press Vessels Pip 87:470–480
25. Chen WQ, Bian ZG, Ding HJ (2004) Three-dimensional vibration analysis of fluid-filled orthotropic FGM cylindrical shells. Int J Mech Sci 46:159–171
26. Vel SS (2010) Exact elasticity solution for the vibration of functionally graded anisotropic cylindrical shells. Compos Struct 92:2712–2727
27. Sladek J, Sladek V, Krivacek J, Zhang C (2005) Meshless local Petrov-Galerkin method for stress and crack analysis in 3-D axisymmetric FGM bodies. CMES Comput Model Eng Sci 8:259–270
28. Sladek J, Sladek V, Tan CL, Atluri SN (2008) Analysis of transient heat conduction in 3D anisotropic functionally graded solids by the MLPG method. CMES Comput Model Eng Sci 32:161–174
29. Sladek J, Sladek V, Solek P (2009) Elastic analysis in 3D anisotropic functionally graded solids by the MLPG. CMES Comput Model Eng Sci 43:223–252
30. Tornabene F, Fantuzzi N, Ubertini F, Viola E Strong formulation finite element method based on differential quadrature: a survey. Appl Mech Rev 67:020801-1-55
31. Alibeigloo A, Nouri V (2010) Static analysis of functionally graded cylindrical shell with piezoelectric layers using differential quadrature method. Compos Struct 92:1775–1785
32. Akbari Alashti R, Khorsand M, Tarahhomi MH (2013) Thermo-elastic analysis of a functionally graded spherical shell with piezoelectric layers by differential quadrature method. Scientia Iranica 20:109–119
33. Asanjarani A, Satouri S, Alizadeh A, Kargarnovin MH (2015) Free vibration analysis of 2D-FGM truncated conical shell resting on Winkler-Pasternak foundations based on FSDT. Proc Inst Mech Eng Part C J Mech Eng Sci 229:818–839
34. Bahadori R, Najafizadeh MM (2015) Free vibration analysis of two-dimensional functionally graded axisymmetric cylindrical shell on Winkler-Pasternak elastic foundation by First-order Shear Deformation Theory and using Navier-differential quadrature solution methods. Appl Math Model 39:4877–4894
35. Jodaei A, Jalal M, Yas MH (2012) Free vibration analysis of functionally graded annular plates by state-space based differential quadrature method and comparative modeling by ANN. Compos Part B Eng 43:340–353
36. Hosseini-Hashemi Sh, Akhavan H, Taher H Rokni Damavandi, Daemi N, Alibeigloo A (2010) Differential quadrature analysis of functionally graded circular and annular sector plates on elastic foundation. Mater Design 31:1871–1880
37. Wu L, Wang H, Wang D (2007) Dynamic stability analysis of FGM plates by the moving least squares differential quadrature method. Compos Struct 77:383–394
38. Leissa AW (1969) Vibration of Plates, NASA SP-160, Washington
39. Leissa AW (1973) Vibration of Shells, NASA SP-288, Washington
40. Werner S (2004) Vibrations of shells and plates, 3rd edition: revised and expanded. CRC Press, Marcel Dekker Inc., New York
41. Brischetto S, Carrera E (2010) Importance of higher order modes and refined theories in free vibration analysis of composite plates. J Appl Mech 77:1–14
42. Tornabene F, Brischetto S, Fantuzzi N, Viola E (2015) Numerical and exact models for free vibration analysis of cylindrical and spherical shell panels. Compos Part B Eng 81:231–250
43. Brischetto S (2014) Three-dimensional exact free vibration analysis of spherical, cylindrical, and flat one-layered panels. Shock Vib 2014:1–29
44. Brischetto S (2014) An exact 3D solution for free vibrations of multilayered cross-ply composite and sandwich plates and shells. Int J Appl Mech 6:1–42
45. Brischetto S, Torre R (2014) Exact 3D solutions and finite element 2D models for free vibration analysis of plates and cylinders. Curved Layer Struct 1:59–92
46. Brischetto S (2014) A continuum elastic three-dimensional model for natural frequencies of single-walled carbon nanotubes. Compos Part B Eng 61:222–228
47. Brischetto S (2015) A continuum shell model including van der Waals interaction for free vibrations of double-walled carbon nanotubes. CMES Comput Model Eng Sci 104:305–327
48. MSC Nastran, Products (http://www.mscsoftware.com/product/msc-nastran. Accessed 20th May 2015
49. Tornabene F, Viola E (2009) Free vibration analysis of functionally graded panels and shells of revolution. Meccanica 44:255–281
50. Tornabene F, Viola E (2009) Free vibrations of four-parameter functionally graded parabolic panels and shells of revolution. Eur J Mech A Solids 28:991–1013
51. Tornabene F (2009) Free vibration analysis of functionally graded conical, cylindrical shell and annular plate structures with a four-parameter power-law distribution. Comput Methods Appl Mech Eng 198:2911–2935
52. Tornabene F, Viola E, Inman DJ (2009) 2-D differential quadrature solution for vibration analysis of functionally graded conical, cylindrical shell and annular plate structures. J Sound Vib 328:259–290
53. Tornabene F, Liverani A, Caligiana G (2011) FGM and laminated doubly-curved shells and panels of revolution with a free-form meridian: a 2-D GDQ solution for free vibrations. Int J Mech Sci 53:446–470

54. Tornabene F, Ceruti A. (2013) Mixed Static and dynamic optimizazion of four-parameter functionally graded completely doubly-curved and degenerate shells and panels using GDQ method. Math Prob Eng. Article ID 867079, 1–33
55. Tornabene F, Fantuzzi N, Bacciocchi M (2014) Free vibrations of free-form doubly-curved shells made of functionally graded materials using higher-order equivalent single layer theories. Compos B Eng 67:490–509
56. Tornabene F, Viola E, Fantuzzi N (2013) General higher-order equivalent single layer theory for free vibrations of doubly-curved laminated composite shells and panels. Compos Struct 104:94–117
57. Tornabene F, Viola E (2013) Static analysis of functionally graded doubly-curved shells and panels of revolution. Meccanica 48:901–930
58. Tornabene F, Reddy JN (2013) FGM and laminated doubly-curved and degenerate shells resting on nonlinear elastic foundation: a GDQ solution for static analysis with a posteriori stress and strain recovery. J Indian Inst Sci 93:635–688
59. Tornabene F, Fantuzzi N, Viola E, Batra RC (2015) Stress and strain recovery for functionally graded free-form and doubly-curved sandwich shells using higher-order equivalent single layer theory. Compos Struct 119:67–89
60. Tornabene F, Fantuzzi N, Bacciocchi M, Viola E (2015) Accurate Inter-laminar recovery for plates and doubly-curved shells with variable radii of curvature using layer-wise theories. Compos Struct 124:368–393
61. Soedel W (2005) Vibration of Shells and Plates. Marcel Dekker Inc, New York
62. Carrera E, Brischetto S, Nali P (2011) Plates and shells for smart structures: classical and advanced theories for modeling and analysis. Wiley, New Delhi
63. Tornabene F, Fantuzzi N (2014) Mechanics of laminated composite doubly-curved shell structures. The generalized differential quadrature method and the strong formulation finite element method, Società Editrice Esculapio, Bologna (Italy)
64. Hildebrand FB, Reissner E, Thomas GB (1949) Notes on the foundations of the theory of small displacements of orthotropic shells, NACA Technical Note No. 1833, Washington
65. Gustafson GB. Systems of differential equations. http://www.math.utah.edu/gustafso/, Accessed 16 September 2014
66. Boyce WE, DiPrima RC (2001) Elementary differential equations and boundary value problems. Wiley, New York
67. Zwillinger D (1997) Handbook of differential equations. Academic Press, New York
68. Molery C, Van Loan C (2003) Nineteen dubious ways to compute the exponential of a matrix, twenty-five years later. SIAM Rev 45:1–46
69. Messina A. Three dimensional free vibration analysis of cross-ply laminated plates through 2D and exact models, 3rd International conference on integrity, reliability and failure, Porto (Portugal), 20–24 July 2009
70. Soldatos KP, Ye J (1995) Axisymmetric static and dynamic analysis of laminated hollow cylinders composed of monoclinic elastic layers. J Sound Vib 184:245–259